Desalination 625 (2026) 119942

Contents lists available at ScienceDirect

Desalination

journal homepage: www.elsevier.com/locate/desal

Renewable energy powered membrane technology: Resilient operating windows of a photovoltaic-powered desalination system operating under transient solar conditions

Emmanuel O. Ogunniyi, Bryce S. Richards *

Institute of Microstructure Technology (IMT), Karlsruhe Institute of Technology, Hermann-von-Helmholtz-Platz 1, 76344, Eggenstein-Leopoldshafen, Germany

HIGHLIGHTS

- PV-membrane pump resilient to shutdowns at low *TMP* set-point/high PV power
- PV power deviations thresholds investigated for pump resilience boundary
- Defined resilient operating windows for PV-membrane under transient operation
- Enhanced resilience with control increases daily production with no energy buffering
- Real-world demonstration ⇒ optimal membrane configuration under transient operation

GRAPHICAL ABSTRACT

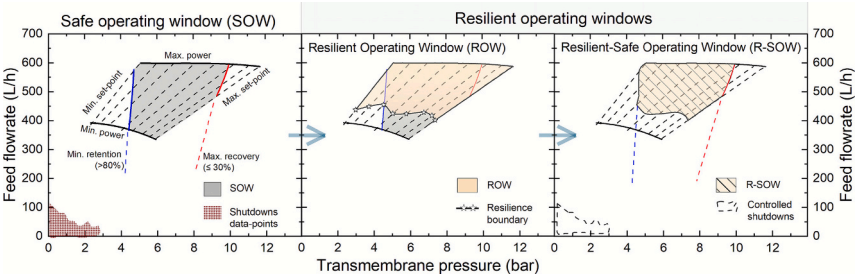

ARTICLE INFO

Keywords:
Control
Reverse osmosis
Nanofiltration
Operating window
Photovoltaics
Resilience
Shutdowns

ABSTRACT

A photovoltaic-powered membrane filtration (PV-membrane) system desalinates brackish water to produce drinkable water using sunlight but is prone to shutdowns – due to solar irradiance fluctuations – that reduce permeate quality and daily yield. Shutdowns occur at certain PV power deviation thresholds ($\mathscr{D}_{\mathscr{M}}$) that, when identified, can be controlled to operate the system autonomously within certain windows of shutdown resilience during transient operation. This study introduces the resilient operating window (ROW) to investigate PV-membrane system operation under four different configurations – via two membranes (BW30 & NF90) and two pumps (SQFlex 0.6-3 N/20 bar & -2 N/12 bar) – using real-world solar conditions. The BW30/3 N configuration, operated at ~11 bar transmembrane pressure (*TMP*), achieved ~67% shutdown resilience while the NF90/3 N configuration at ~9 bar *TMP* (constrained) achieved 100% resilience & daily production gains of 8 L and 19 L, respectively, compared to reference uncontrolled operation. The -2 N pump enabled 100% resilience for both membranes, with reduced daily yield for NF90. Results highlight how $\mathscr{D}_{\mathscr{M}}$ influences shutdowns in PV-membrane systems, and how these can be mitigated for enhanced resilient operation during transient conditions without additional energy buffering support, essential for more robust autonomous PV-membrane water desalination systems.

* Corresponding author.
E-mail address: bryce.richards@kit.edu (B.S. Richards).

https://doi.org/10.1016/j.desal.2026.119942
Received 9 November 2025; Received in revised form 30 January 2026; Accepted 2 February 2026
Available online 3 February 2026

1. Introduction

To optimally operate a photovoltaic-powered membrane (PV-membrane) desalination system, it is essential to fully utilise the available PV power at every instance of the day to enhance daily water production [1–3], while ensuring the permeate quality is within the palatable limits of drinking water. The palatability of water with total dissolved solids (TDS) <0.6 g/L is generally considered to be good; drinking water becomes increasingly unpalatable at TDS levels >1 g/L and beyond this limit is not recommended [4].

In prior studies, a "safe operating window" (SOW) concept was defined for wind- and PV-powered membrane desalination systems. This helped to determine the membrane optimal operating thresholds under a steady-state condition using constant power supply [5–8]. In real-world scenarios, PV-membrane systems rarely operate under steady-state conditions due to continuous solar irradiance (SI) fluctuations during clouds movement, which cause power and pressure variations in PV-membrane system. In extreme cases, there is intermittency where PV power can drop sharply enough to trigger PV-membrane pump shutdowns.

This study thus extends the SOW concept and introduced two significant operating windows of a PV-membrane system under transient operation, applicable to real-world operation: The resilient operating window (ROW) and resilient safe operating window (R-SOW). These resilience-based windows are defined through empirically identified PV power deviation thresholds ($\mathscr{D}_{\mathscr{M}}$) where pump shutdowns occur across a range of transmembrane pressure (*TMP*) demands in PV-membrane system. The $\mathscr{D}_{\mathscr{M}}$ are the maximum allowable instantaneous change in PV power per second, beyond which the pump-drive system becomes electrically unstable, and its internal logic initiates a protective shutdown.

The conceptual distinction of these new windows, further definitions and motivation of the study are presented in this section.

1.1. Conceptual difference between SOW, ROW and R-SOW for PV-membrane system

The SOW concept – originally proposed by Feron in 1985 [5] – has been furthermore investigated under steady-state conditions [5–8]. The window is determined by plotting the feed flowrate against the transmembrane pressure (*TMP*). The region is then mapped out under different constraints which combines the hydraulic, electrical, and membrane-performance characteristics of the system. These are: ① minimum retention to attain drinkable permeate; ② minimum pump power, such that the pump can produce a flow at each pressure set-point; ③ minimum and maximum pressure set-points; ④ maximum recovery to reduce the fouling risk, and ⑤ maximum pump power across each *TMP* set-point. An example of a SOW is illustrated in Fig. 1A.

The SOW (the grey shaded area where all the aforementioned constraints are simultaneously satisfied to produce safe drinking water) helps to identify retention, recovery, flux, specific energy consumption (*SEC*), TMP demand, and pump power under steady-state power supply. It does not however indicate whether an operating point will survive transient PV power fluctuations, or when shutdown mitigation is required.

The ROW introduces a PV power deviation resilience limit, which helps to determine pump tolerance, enabling the prediction of whether a given operating point will trigger pump shutdown under transient photovoltaic conditions. The ROW overlays dynamic power variability onto the SOW and, unlike the SOW, identifies quantifiable PV power deviation thresholds at which pump shutdowns occur during transient operation, applicable to real-world PV-membrane applications.

A typical ROW is shown in Fig. 1B, and it is defined under the following constraints: ①minimum set-point, ② resilience boundary, ③maximum set-point, ④ maximum pump power.

The resilience boundary is derived from empirically determined $\mathscr{D}_{\mathscr{M}}$. Specifically, within the ROW, $\mathscr{D}_{\mathscr{M}}$ are not sufficient to trigger the pump shutdown, meaning that no buffering or shutdown control strategy may be required. Below the ROW however, the $\mathscr{D}_{\mathscr{M}}$ can potentially result in pump shutdown depending on the severity of the power variations.

Because the ROW alone does not ensure that the system operates strictly within the membrane's safe boundaries defined by the SOW, a resilient safe operating window (R-SOW) is defined. R-SOW identifies operating regions where both membrane safety and shutdown resilience are simultaneously satisfied. It applies the same resilience conditions of the ROW in addition to the SOW boundaries. As shown in Fig. 1B, the R-SOW represents the intersection between the SOW and the ROW, highlighting the region where PV-membrane operation can be both "safe" and "resilient" under real-world transient PV conditions.

Typically, for feed brackish water with total dissolved solids (TDS) of 5 g/L, a minimum retention of 80% is required to attain a 1 g/L permeate, and maximum recovery of ~30% is recommended to reduce

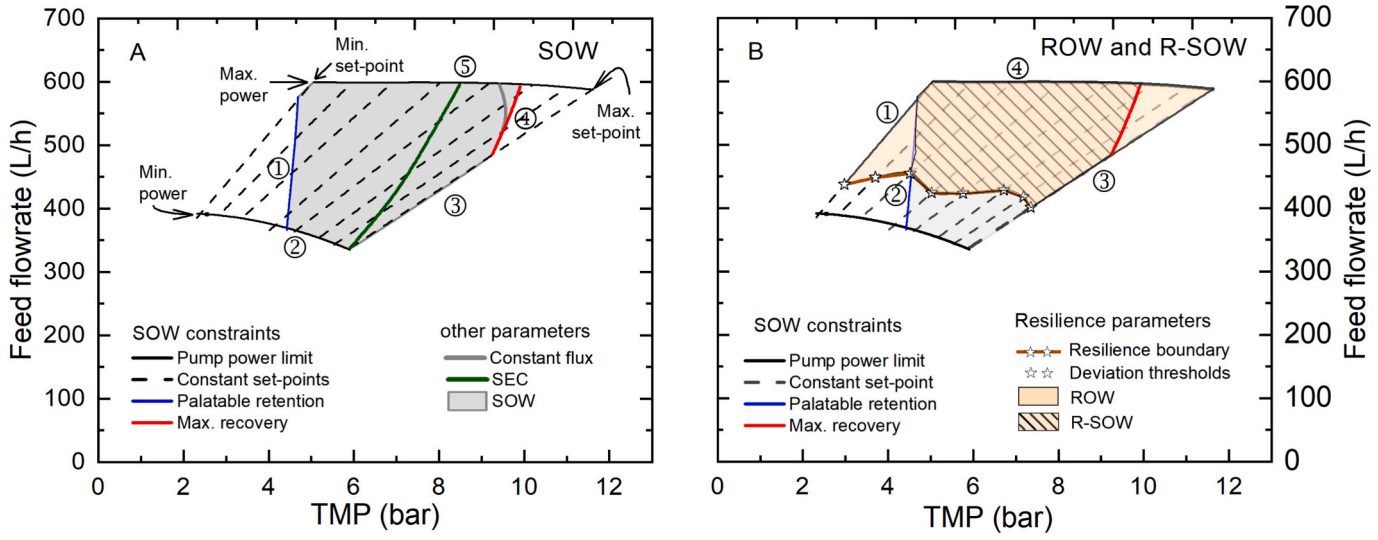

Fig. 1. Different operating windows of a photovoltaic-powered membrane filtration system. A. The original steady-state safe operating window (SOW) with its boundary defined by the constraints: ① palatable retention, ② minimum pump power, ③ maximum pump power, ④ maximum pressure set-point ⑤ maximum recovery; B. Proposed resilient operating window (ROW) for transient operation along with the resilient-safe operating window (R-SOW), defined as the overlap of the SOW and ROW. ROW and R-SOW are bounded by: ① minimum set-point, ② resilience boundary, ③ maximum set-point, and ④ maximum pump power.

the fouling risk and preserve the membrane integrity. Although membrane desalination of brackish water can attain a higher recovery of >30%, this is mostly reported for multi-stage operation consisting of an additional circulation pump [9–11], or a single-pass system consisting of multiple spiral-wound elements (SWEs) up to eight, in series within a single pressure vessel. For experimenting with a single SWE, the recommended recovery rate is provided by the membrane manufacturer. For example, *DuPont* recommend operating single SWE (BW30–4040 or NF90–4040) at a low recovery of ~25% [12], which helps to minimise scaling or fouling rate during continuous operation. This also keeps the membrane performance within the "sustainable flux" limit [13] also referred to as the threshold flux or sustainable critical flux [14,15] – and defined as being the operating limit where flux is high enough for permeate production, but low enough to keep fouling at manageable levels.

1.2. PV-membrane pump and shutdown dynamics

Positive displacement pumps (PDPs), consisting of progressive cavity, are mostly used in PV-membrane desalination systems as they are designed to generate high pressure at relatively low flow rate, a matching profile for pressure-driven membrane desalination processes [16]. The other pump category – dynamic pumps (e.g. centrifugal pump) are however more suited to applications requiring high flow rates at low pressures (e.g. irrigation) [17]. Progressive cavity PDPs share similar helical rotor-stator displacement mechanism, and so they are comparable in operation and shutdown dynamics.

The pump shutdown, which mainly result from electrical stress from voltage fluctuations or unbalanced currents, can occur under two conditions: i) Motor stalling [18] – when the power drops too low and the motor torque becomes insufficient to overcome the pump's load (the pressure of lifting water); ii) Electronic protection – Modern controllers have (built-in) power control unit which protects the pump from rapid power fluctuations [19,20]. Once the magnitude of the input power fluctuation exceeds the level required for stable motor operation, the controller logic triggers a shutdown. The corresponding $\mathscr{D}_{\mathscr{M}}$ at shutdown therefore defines the pump's resilience boundary which can be empirically determined.

Although this study does not aim to characterise or compare the intrinsic shutdown thresholds of different pump types or models, it recognises that most modern PV-powered pumps incorporate defined, and often pump-specific, protection limits that can be empirically identified. However, once these thresholds are determined (empirically), the critical question shifts from why or how the shutdowns occur to how such thresholds can be strategically utilised in PV-membrane systems control, to improve the system operational stability and daily production.

Pump shutdowns are undesirable in PV-driven membrane systems for three reasons. Firstly, during a shutdown period, the permeate quality deteriorates [21] due to the reduction of the hydraulic driving force, allowing back-diffusion of salts from the concentrated feed to the permeate side. Secondly, frequent shutdowns throughout a solar day can significantly increase the *SEC,* because energy is repeatedly expended during non-productive start-up and re-pressurisation phases, while permeate production only occurs after sufficient pressure is re-established. In addition, due to continuous interruption of permeate production during the pump downtime, there is reduction of cumulative daily production [22,23].

1.3. Power flow process of PV-powered positive displacement pump

In modern PV-powered pumps with integrated electronics, the inbuilt maximum power point tracking (MPPT) controller continuously adjusts the operating point of the power converter to maximise energy extraction from a fluctuating PV supply. Continuous MPPT (e.g. during heavy cloud passage) repeatedly reconfigures the DC converter operating states, which can cause transient undervoltage or current overshoot [24]. The commutator then converts the DC supply (or rectified AC) into time-varying current in each stator winding of the motor. A block diagram of this typical power flow process for a (helical rotor) progressing cavity PDP [17,25,26] in PV-membrane system is shown in Fig. 2. The motor rotational speed is proportional to the available electrical power supply, while the torque increases linearly with pressure demand and notably almost independent of speed (unlike centrifugal pumps, where torque increases with speed).

When the internal controller detects that stable motor commutation cannot be guaranteed, the embedded control logic disables the commutator, which shuts down the motor at the preprogrammed resilience threshold of the pump. A permanent magnet synchronous motor is mostly used for helical rotor PDP as it is suitable for constant-torque loads with no slip losses. This controlled shutdown, which protects the pump from accelerated ageing due to mechanical stress or overcurrent conditions [27] is defined using Eq. (1):

$$\left.\begin{array}{l} V_{PV}(t) > V_{pump,\,min} \\ P_{PV}(t) > P_{pump,\,min} \end{array}\right\}_{running\ condition;\ no\ shutdown} \quad \left.\left|\frac{dP_{pv}}{dt}\right| > \left(\frac{dP_{pump.max}}{dt}\right)\right|_{possible\ stalling;\ shutdown} \tag{1}$$

where: $V_{PV}(t)$, $P_{PV}(t)$ = instantaneous PV voltage and power supply respectively; $V_{pump,min}$, $P_{pump,min}$ = minimum operating thresholds of the pump voltage and pump power respectively; $\left|\frac{dP_{pv}}{dt}\right|$ = absolute magnitude of PV power fluctuations, $\frac{dP_{pump.max}}{dt}$ = maximum tolerable pump power fluctuations.

Since pump controllers are designed to shut down under fast power deviations, system-level strategies that smooth power demand rather than modifying internal electronics are essential.

1.4. Shutdowns mitigation strategies for PV-membrane system

To optimise PV-membrane system performance for transient conditions (e.g. fluctuations over the timeframe of seconds), it is important to mitigate the risk of pump shutdowns. A common approach for achieving this is via the addition of energy storage components to the system. This was demonstrated for a wind-powered membrane filtration system, whereby supercapacitors (SCs) smoothed out power fluctuations for up to 5 h, which resulted in the system operating within the SOW for a significantly greater fraction of time [28]. Likewise, with the integration of power control management system into a PV-membrane system, energy buffering with a high energy density SC extended the operating time to multiple days [23]. However, the simplicity of directly-coupled PV-membrane systems – i.e. where no energy storage components are included – have advantages when it comes to robustness [16], an important attribute when such systems being deployed in harsh environments and remote locations [29].

An alternative approach is to implement a control strategy to directly mitigate the pump shutdowns directly without additional energy buffering option. This can make the PV-membrane system more robust for directly-coupled operation, while avoiding challenges associated with energy-storage options, including conversion losses, maintenance requirements, and periodic replacement. In a prior study, the present authors investigated this approach for PV-membrane system desalinating brackish water containing 5 g/L NaCl TDS, using a single pump operated at a fixed *TMP* set-point of 12 bar [30]. The system back-pressure was controlled using an actuator and integrated ball valves at $\mathscr{D}_{\mathscr{M}}$ of 30%/s where the electrical shutdown of the helical rotor PDP occurred. This effectively minimised the pump shutdown occurrences, especially on a very cloudy day. Inspired by this result, and the motivation to extend this approach to other pump-membrane configurations,

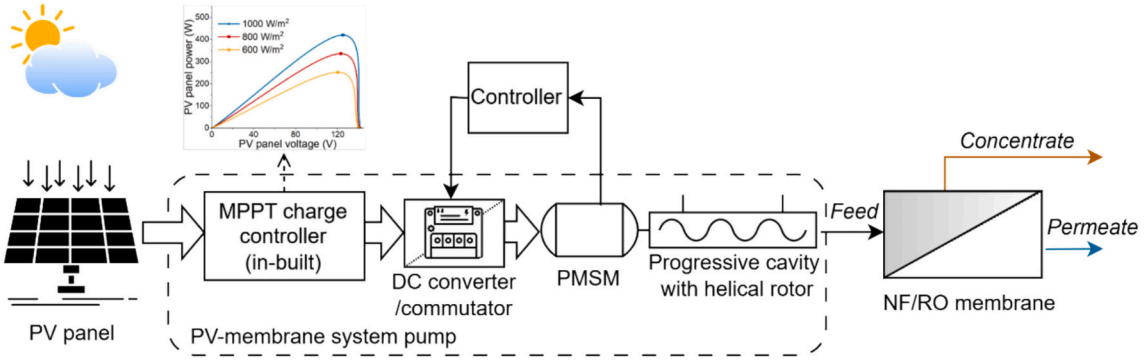

Fig. 2. Block diagram of power flow process for PV-powered pump for membrane desalination system. NF = Nanofiltration, PMSM = Permanent magnet synchronous motor; RO Reverse Osmosis.

the current study seeks to i) explore the temporal dynamics of PV-membrane system under transient power supply, ii) identify the thresholds of PV power fluctuations that trigger system shutdowns across different *TMP* set-points and PV power supply ranges; and, subsequently, iii) define the ROW and R-SOW of the system under such transient conditions which can further provide a guide for the control similar PV-membrane systems to achieve resilient operation.

Thus, explore these, the following research questions were investigated:

i. How do PV power $\mathscr{D}_{\mathscr{M}}$ vary across different *TMP* and PV power levels in a directly-coupled PV-membrane system, and how do these affect the shutdown and resilience dynamics in different pump-membrane configurations?
ii. How can the $\mathscr{D}_{\mathscr{M}}$ be mapped onto a SOW to identify the region of ROW where the system can be resilient to shutdowns across different *TMP* set-points during transient operation?
iii. How can R-SOW of PV-membrane be determined, such that the system operate within the SOW boundary conditions, while maintaining the shutdown resilience, applicable for real-world application?

2. Materials and methods

2.1. Clarifications of key terms and concepts

2.1.1. PV power ramp rate versus PV power deviation thresholds

When a system operates under transient SI conditions, it is subjected to PV power fluctuations, often quantified in terms of PV power ramp rates (RR) – defined as the (absolute) rate of change of PV power supply with time (units: W/s) [31,32]. System shutdowns in a PV-membrane system can occur when the PV power RR exceeds a certain magnitude [21], however, the impact of RR magnitude under different PV power levels is not uniform on such system. For instance, a 100 W/s ramp down magnitude can cause a pump shutdown at low power (e.g. from 300 W to 200 W in 1 s) may be tolerated by the same system under high power supply (e.g. 600 W to 500 W in 1 s). Although the RR magnitude is the same, the occurrence under low PV power condition could bring the pump below its "shut-off" limit, while this may be tolerated under the higher PV power condition.

PV power $\mathscr{D}_{\mathscr{M}}$ are relevant for enabling a consistent threshold across different SI conditions,. This is defined in terms of the rate of change of PV power supply, referenced to the previous output value (units: %/s). It indicates the percentage disturbance relative to instantaneous system conditions, which can be applicable to different operating *TMP* set-points or PV power levels. Although several studies have reported the behavior of PV-membrane under PV-power fluctuations [3,21,33–37], the quantitative $\mathscr{D}_{\mathscr{M}}$ at which pump shutdowns occur have not been much reported, as these depend on different factors, such as the pump's dynamic response, operating pressure, available PV power, and membrane type.

2.1.2. Membrane resilience versus pump resilience to shutdowns

In previous studies, membrane resilience is defined as the time required for the key performance indicators (e.g. flux, permeate conductivity) to recover to their pre-disturbance levels following a disruption such as a system shutdown [21,38]. This time-based definition assumes that the PV power supply remains relatively unchanged before and after the disruption, and that system performance is capable of fully returning to its initial state. Classical definitions of resilience are often based on a normal operating state, a disrupted state, and then recovery to the initial state after a period of time [39]. The time-based resilience definition is however difficult to apply to a solar day that is characterised with high SI fluctuations, since the system performance may not always fully recover to the initial level post disruption. In PV-membrane system, however, the pump supplies the needed hydraulic pressure to the membrane, thus the pump resilience to shutdown is more applicable for system investigation under transient operation.

Pump resilience is defined in this study as the pump's ability to withstand PV power fluctuations without shutting down under PV power transient condition. For a fixed PV array size, membrane type, back-pressure setting and the membrane *TMP* set-point, this is expressed as the maximum tolerable PV power $\mathscr{D}_{\mathscr{M}}$ that the pump can absorb while continuing stable operation for a fixed system design. Low resilience indicates that the pump is prone to shutdowns under relatively small fluctuations in PV power supply, while high resilience is the ability of the pump to withstand larger degrees of fluctuation without shutdown.

2.2. PV-membrane system set up and descriptions

The resilient operation of PV-membrane system under transient PV power supply was investigated using two helical rotary pumps with different maximum operating pressure limits: 12 bar and 20 bar. The effects of membrane performance during this transient operation on a cloudy day was assessed using two membrane types, one nanofiltration (NF) membrane and one brackish water RO membrane. The schematic representation of the system set up is shown in Fig. 3, while the complete system setup and description are summarised below.

2.2.1. PV panel / solar array simulator

The system utilised six silicon PV modules (OffgridTec) with the following specifications: Maximum power on load (P_{mp}) = 100 W, voltage at maximum power (V_{mp}) = 39.6 V, current at maximum power (I_{mp}) = 2.53 A, temperature coefficient $\beta = -0.45\%/°C$ and surface area = 0.575 m^2). These are conFig.d in a 3-series × 2-parallel arrangement, to produce a maximum power of $P_{mp} = 600$ W ($V_{mp} = 118.8$ V $I_{mp} =$ and 5.06 A) at standard test conditions of 1000 W/m^2 SI and 25 °C. The configuration was selected to match the DC power requirements of the

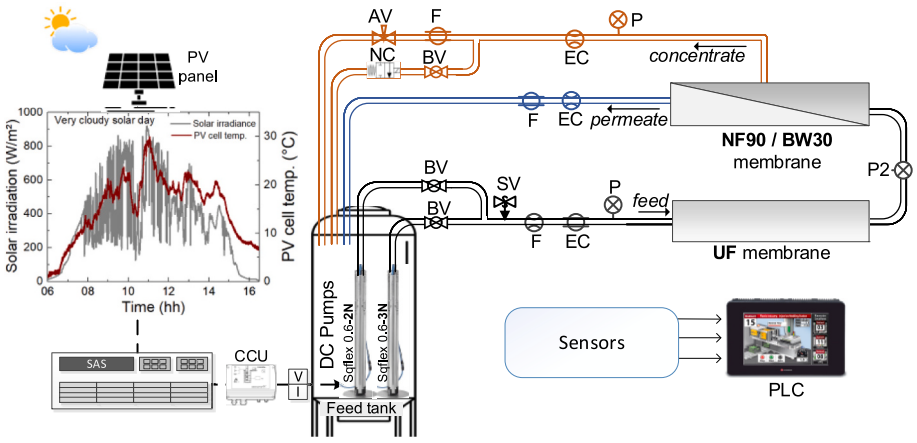

Fig. 3. PV-membrane system set-up for resilience investigation during transient PV power supply, showing: a very cloudy day used as the solar irradiance input to the solar array simulator (SAS); the choice of two pumps submerged in the feed tank (containing 5 g/L NaCl)– SQFlex 0.6-2 N, SQFlex 0.6-3 N; and the choice of two membranes for desalination – BW30 and NF90. AV = Actuator valve, BV = Ball valve, CCU = Control and communication unit, CV = Check valve, EC = Electrical conductivity sensor, F=Flow sensor, NC=Normally closed solenoid valve, P=Pressure sensor, PLC = Programmable logic controller, SAS=Solar array simulator, SV=Safety valve.

chosen pumps (detailed in next subsection). To ensure reproducibility of a solar day for different experimental testing in the laboratory, the PV array was emulated using a solar array simulator (SAS, Chroma 62050H—600S, 5 kW DC supply), programmed with specific SI and temperature profiles. The SI dataset obtained from 2016 measurements at the KIT Solar Park, Germany was programmed into the SAS. A very cloudy day (13 October 2016) – plotted on the left in Fig. 3 – was used in the study to investigate system resilience. This day is particularly applicable as it represents a near worst-case scenario of multiple levels SI fluctuations. In addition to transient power supply, the SAS can be programmed to supply constant DC power, which is needed for steady-state experiments.

2.2.2. Feed pump and control unit

Two submersible DC-powered helical rotor pumps with different maximum pressure limits were used interchangeably. These are Grundfos: SQFlex 0.6-2 N (maximum pressure 12 bar, ~420 W) and SQFlex 0.6-3 N (maximum pressure 20 bar, ~600 W) and both pumps are capable of a maximum feed flow rate of 600 L/h [25,26]. Although both pumps can be operated to supply the same feed pressure under identical power supply, their resilience to PV power fluctuations may differ due to variations in their maximum power demand, which can influence their effective operating range before shutdown. Due to these differences, the pumps were selected to investigate how their maximum pressure limit affects the system shutdowns and resilience. These pumps are connected to the power source via the control and communication unit (CCU) CU200 by Grundfos.

2.2.3. Membranes

Three membranes were used in the system: i) an ultrafiltration (UF) membrane (Inge Dizzer P4040, 6.0 m^2) was always employed for feed-water pre-treatment. Then for for brackish water desalination, a choice of two membranes could be used, either ii) a RO membrane (DuPont FilmTec BW30–4040, 7.2 m^2) [40]. The BW30 membrane in the system is relatively old (in use for about 3 years), offering a maximum salt rejection of about 93%; or iii) a NF membrane (DuPont FilmTec NF90–4040, 7.6 m^2), which selectively removes multivalent ions and organics while allowing monovalent ions to pass, achieving up to 95% rejection. The NF90 membrane provides higher flux and serves as an alternative to BW30 for evaluating system performance and effects on the pump's resilience to system shutdown.

2.2.4. The Transmembrane pressure (TMP)

The *TMP* is the study is the effective feed pressure measured at the inlet of the desalination membranes (NF90 or BW30), following pre-treatment via the UF membrane. This *TMP* is slightly lower (~0.8 bar drop) than the feed pressure due to the pressure drop in the UF membrane.

2.2.5. Feed water, quality and temperature

The feed water is a synthetic brackish water consisting of a de-ionised water and 5 g/L NaCl (> 99%, Sigma-Aldrich, general-purpose grade). The feedwater temperature was regulated using a water circulation chiller (Julabo FC-600, Germany) connected to the interlayer of the 270 L custom-built, double-walled feed tank used in the setup. The chiller allowed feedwater temperature to be controlled to about 20.5 ± 0.5 °C for all the experiments.

2.2.6. Control, valves and sensors

A programmable logic controller (PLC, Unistream 10.4″, Unitronics) was employed to regulate the power supply and overall performance of the PV-membrane system. The PLC can process up to 40 analogue signals (4–20 mA) from sensors. The sensors in the system include pressure transmitters, electrical conductivity sensors, flow sensors, DC current transducers, and uni−/bipolar DC voltage transmitters. The analogue and digital outputs of the PLC were respectively used to control the electrical actuator valve (Hanbay MCL-S50 AB 24 V SS) and solid-state relays (TRU-components TC-GSR-1-40DD) used for switching operations within the system. Detailed descriptions and types of the sensors and valves have been presented in previous work [30], as the present system builds on similar configuration with modifications in pumps and control methods.

2.3. Determining the operating windows of PV-membrane system

The operating windows of a PV-membrane system define the ranges of conditions under which the system can function effectively, both in terms of safety and resilience. The operating windows considered are the: SOW, ROW and R-SOW. The methods of determining these operating windows are described in this section.

2.3.1. Steady-state test and SOW

The SOW is determined through a series of performance tests conducted under steady-state conditions (that is, constant power supply and fixed operating setpoints). The steady-state results are subsequently

used to map out the SOW, which is realised by first plotting the feed flow rates against the corresponding effective feed pressure. In the study, the SOW investigation is carried out as follows:

i. A *TMP* value (e.g., 12 bar) is set using the maximum PV power supply of $P_{mp} = 550$ W.
ii. The back-pressure valve position is fixed to maintain the *TMP*, and the constant power supply is varied from 200 W to 550 W in 50 W increments. For each power level, the system operates for 10–20 min under steady power supply until the system performance is stabilised.
iii. After completing the power variation, the next *TMP* value (e.g., 11 bar) is set using the maximum power of 550 W. The power is then likewise varied from 200 W to 550 W in 50 W increments, following the same steady-state procedure.
iv. PV power supply limits of 200–550 W were chosen because 550 W is the practical maximum power supply from the PV panel configuration, while below 200 W the pump a) can no longer generate sufficient *TMP* for the PV-membrane system to produce permeate and b) is prone to inevitable shutdown, the exact limit depends on the pump type.
v. The steps above are repeated until all operating pressure set-points from 12 bar down to 5 bar are investigated (in 1 bar intervals).
vi. The performance graphs of the parameters are then plotted to see how the individual parameter (flux, retention, feed flow, recovery, *SEC*) changes with the changing power levels and the operating pressure.
vii. These results are then merged and mapped out into a SOW, which is derived by plotting the feed flow rate against the *TMP* in the system (as described earlier in Fig. 1A). The SOW is constrained by the desired thresholds (maximum and minimum power limits, pressure set-points, maximum recovery, minimum retention) and plotted.

2.3.2. Transient-state test, ROW and R-SOW

Transient-state tests were used to determine the ROW while the overlap of the ROW and the corresponding SOW of the same setup are mapped out to determine the R-SOW (as previously illustrated in Fig. 1B). The transient tests involve investigating different magnitudes of $\mathscr{D}_{th}$ that can either trigger pump shutdown or be tolerated by PV-membra ne system under various operating *TMP* set-points. PV power fluctuations was investigated in terms of $\mathscr{D}_{th}$, instead of ramp rates in W/s, since the units of %/s provides more consistent comparison across different PV power levels or set-points. Since real time PV power fluctuation magnitudes are mostly challenging to predict perfectly due to inherent fast-changing cloud conditions, the $\mathscr{D}_{th}$ are simulated using SAS to generate controlled magnitudes of SI fluctuations in %/s. The method of the $\mathscr{D}_{th}$ identification is carried out as follows:

i. An operating *TMP* (e.g. 12 bar) is set using the maximum power of 550 W. At this set-point, PV power supply levels simulated with different magnitudes of $\mathscr{D}_{th}$, are applied.
ii. The PV power levels are varied from 200 W to 550 W at 50 W increment similar to SOW investigation for better comparison. For each power level, the $\mathscr{D}_{th}$ are varied from 0%/s to 80%/s in steps of 5%/s. An illustration of PV power supply data (at 200 W and 500 W) with simulated fluctuations shown in Supplementary Information Fig. S1.
iii. The pressure set-point is then adjusted (e.g., to 11 bar) using the same maximum power (550 W), and the $\mathscr{D}_{th}$ investigation is repeated. This is done for all operating *TMP*s from 5 to 12 bar.
iv. As the PV power deviation magnitudes change, the maximum thresholds at which the pump shuts down at different *TMP* is determined as the pump resilience threshold (%/s).
v. Since the pump power and pressure are linearly correlated, the PV power fluctuations per second produce an approximately equal magnitude of pressure fluctuations per second in the system, as previously investigated [30].
vi. The magnitudes of $\mathscr{D}_{th}$ where the pump shuts down, are thus applied to the pressure set-points of the SOW. This helps to identify the boundary of the ROW across the investigated operating set-points.

2.4. Real-world demonstration of R-SOW

The real-world demonstration of R-SOW was conducted in two steps: i) operating the PV-membrane system in a directly-coupled configuration using the SOW boundary condition (30% recovery) and ii) subsequently implementing the back-pressure control strategy to mitigate the pump shutdowns when the $\mathscr{D}_{\mathscr{M}}$ exceeds the boundary identified in the ROW of the same system. The investigation used real-world SI conditions of a very cloudy day.

Four configurations were investigated using: Two membranes (BW30 and NF90), and two pumps with different maximum pressure ratings – SQFlex 0.6-2 N (12 bar) and SQFlex 0.6-3 N (20 bar) – to assess how variations in pump pressure tolerance affect system resilience within the same operational modes. For these configurations, two operational modes were examined: i) operation under SOW boundary conditions without shutdown control strategy, and ii) operation within the R-SOW limit with shutdown control strategy. The first mode served as a reference case to evaluate system performance under real-world transient conditions, while the second mode demonstrated the system's ability to maintain resilient operation within the SOW boundaries.

2.5. Control strategy for demonstration of R-SOW for PV-membrane system

The actuator valve and bypass ball valve (shown earlier in the system schematic in Fig. 3) are the primary control components of the PV-membrane system, regulating both system performance and the operating windows. The control strategy enables the setting of the membrane operating set-point within the desired threshold, and it prevents pump shutdown during rapid PV power fluctuations. The closed-loop feedback control strategy for these operations is illustrated in Fig. 4.

As shown in Fig. 4, a recovery threshold set for the operating windows was realised by electrically controlling the closure of the AV via the PLC. The recovery, defined as the desired ratio of the permeate to the feed flow rate e.g. at ~30%, was determined using the maximum power supply to the pump. Recovery can also be set by controlling the *TMP* until the desired set-point is attained. The AV enables precise flow and pressure regulation and maintains a fixed valve position throughout the experiment, offering greater stability and reliability than manual valves. For shutdown control, a pre-determined $\mathscr{D}_{th}$ (%/s) was programmed into the PLC as a reference limit. When PV power fluctuations exceeded this threshold, the bypass valve – installed in parallel with the AV – was momentarily opened through an integrated solenoid valve. This temporary pressure release reduced the back pressure buildup, thereby lowering the load on the pump during ramp-down events at low power supply and preventing pump shutdown.

This shutdown mitigation strategy is implemented as an event-triggered supervisory control using closed-loop feedback of the PV power rate-of-change. The PV power $\mathscr{D}_{th}$ act as the sole tuning parameter and is selected based on the experimentally observed onset of pump shutdown. This design choice ensures reproducibility and straightforward implementation in PLC-based systems without reliance on plant-specific dynamic models.

3. Results and discussion

In this section, the following experimental results are presented: i)

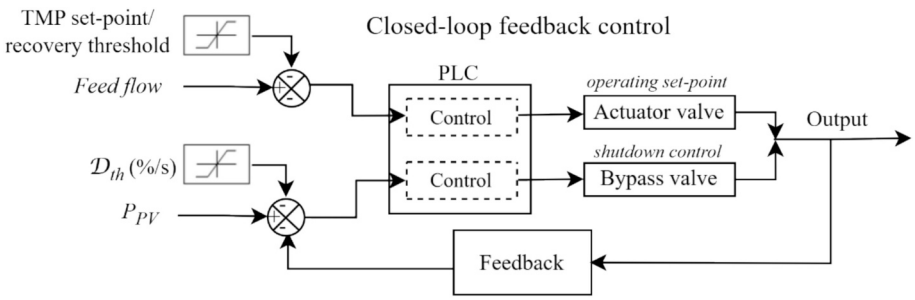

Fig. 4. Closed loop feedback control strategy for real-world application of SOW and R-SOW showing the control strategies for set-point determination and shutdown control during transient PV-membrane system operation.

Determination of SOW, ii) Determination of resilience boundary and ROW; iii) determination of the R-SOW and iv) real-world demonstration of R-SOW. Since the two membranes in the study (BW30 and NF90) have different permeabilities, performance variations are possible and expected. Thus, the analysis and description of the two membranes are presented in this section. For the pump choice, the experimental results with the high-pressure pump (SQFlex 0.6-3 N) are reported in this section while the results with the other pump are provided in the Supplementary Information. This is because both pumps can exhibit comparable performance with the same membrane when operated at identical pressure set-points. In term shutdown resilience, the SQFlex 0.6-3 N is more prone to shutdowns under low power conditions because it demands higher power at low pressure. This makes it particularly suitable for evaluating pump resilience against shutdowns.

3.1. Determination of SOW

This section presents the steady-state results of the experimental investigation of BW30 and NF90 membranes using the SQFlex 0.6-3 N pump. The results were used to map out the SOW boundaries of the corresponding membranes

3.1.1. Steady-state test of BW30 membrane with SQFlex 0.6-3 N pump

The steady-state results of BW30 membrane using SQFlex 0.6-2 N pump are presented in Fig. 5. The relationship between pump power consumption and *TMP* set-point is presented in Fig. 5A. For each set-

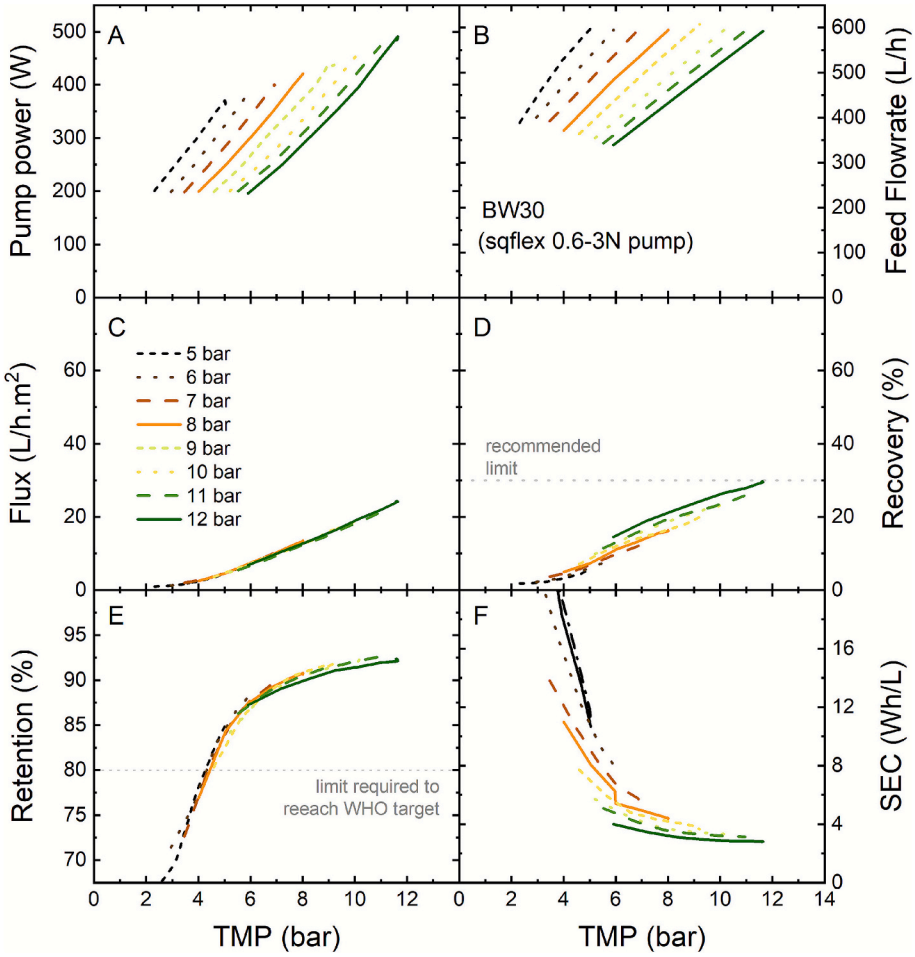

Fig. 5. Performance of the PV-membrane system under steady-state conditions evaluated across 5–12 bar *TMP* (using **BW30** membrane and pump **0.6-3N**): A. pump power, B. feed flowrate, C permeate flux, D. recovery rate, E. salt retention, and F. *SEC*.

point, the pump maximum power consumption increases as the power supply increased until it reached specific thresholds which correspond to the operating *TMP*: for example, ~380 W at 5 bar and ~490 W at the 12 bar. The feed flowrates of the pump at different power demand are shown in Fig. 5B. The minimum feed flowrate corresponding to the minimum power consumption of 200 W, decreased gradually with increasing *TMP*. The flowrates changed approximately linearly with power consumption, reaching a maximum flow of ~600 L/h at the maximum power consumption for each *TMP* set-point. The rate of permeate (drinkable water) production is evaluated in terms of flux and recovery rate: with the BW30 membrane, both parameters recorded their peak supply at the maximum *TMP* of 12 bar, yielding about 24 L/h·m^2 flux (Fig. 5C) and ~ 30% recovery respectively (Fig. 5D). Since the recovery remains below the 30% threshold, this membrane can be safely operated at a *TMP* of 12 bar. A maximum retention of ~93% is realised at the maximum set-point of 12 bar (Fig. 5E), likely due to the age of the BW30 membrane as mentioned earlier in Section 2.2.3 (Membranes). Nevertheless, all investigated set-points (5–12 bar) produce drinkable permeate (>80% retention). The lowest *SEC* of ~3.6 Wh/L is realised at the maximum *TMP* set-point of 12 bar (Fig. 5F).

The same set of results using the SQFlex 0.6-2 N pump are presented in Fig. S2. One notable difference is in the flow characteristics of the pumps. While the feed flowrates are generally higher with 0.6-3 N pump reaching about 600 L/h, the 0.6-2 N pump peaks around ~540 L/h especially at the maximum operating pressure of 12 bar. The pumps experience pressure-induced flow reduction while on load resistance (e.g the membrane *TMP* demand). The 0.6-2 N however is more affected because it's designed for lower throughput, so at high pressure, the flow drop is more noticeable.

3.1.2. *Steady-state test of NF90 membrane with SQFlex 0.6-3 N pump*

The steady-state performance test results of NF90 with SQFlex 0.6-3 N pump are shown in Fig. 6, while the results with SQFlex 0.6-2 N pump are presented in Fig. S3. In Fig. 6A the pump power consumption and *TMP* follow similar trends of correlation as BW30 membrane, while the power supply was varied from 200 to 550 W. This because power consumption is dependent on the operating pressure. Of course, the back-pressure valve needs to be closed further to enable NF90 membrane (due to higher permeability) attain the same *TMP* set-point. At identical pressure set-points, the pump performance becomes comparable for both membrane systems. The corresponding feed flow rates of the pump are shown in Fig. 6B, where the minimum flow rates at 200 W decrease gradually with increasing *TMP*. The flow rates change approximately linearly with power consumption, reaching a maximum of about 600 L/h at the highest power consumption for each *TMP* (Fig. 6B).

The peak outputs of the flux and recovery rate at the maximum *TMP* of 12 bar, yielded about 40 L/h·m^2 flux (Fig. 6C) and ~ 48% recovery respectively (Fig. 6D). The recovery at 12 bar is far greater than the 30% limit desired for the SOW. Thus, for SOW analysis, the PV-membrane system with this pump is operated at a *TMP* ~ 8 bar to attain the desired 30% recovery. A maximum retention of ~95% is realised at the maximum set-point of 12 bar (Fig. 6E). while the lowest *SEC* of ~1.7 Wh/L is realised at the maximum operating pressure of 12 bar (Fig. 6F). Similarly to the performance observed with the BW30 membrane, the SQFlex-0.6-2 N pump investigation with NF90 membrane also experienced greater pressure-induced flow reduction, as shown in Fig. S3. This

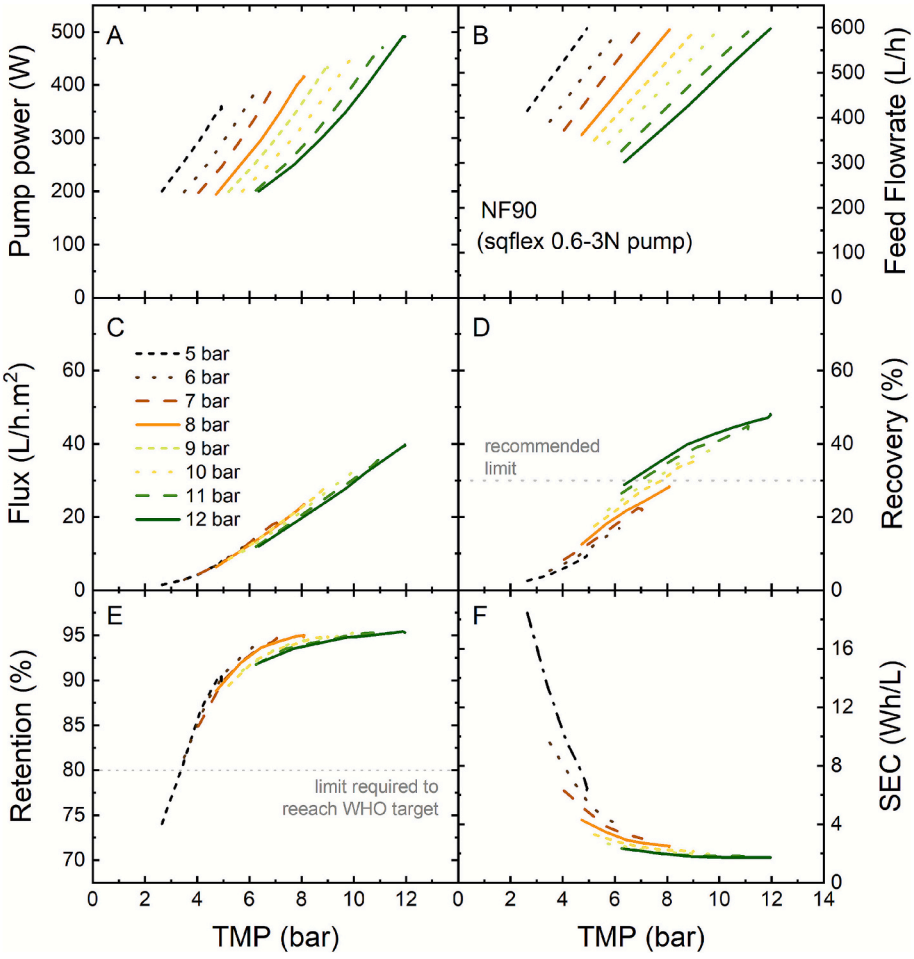

Fig. 6. Performance of the PV-membrane system under steady-state conditions evaluated across 5–12 bar *TMP* (using **NF90 membrane** and pump **0.6-3N**): (A) pump power, (B) feed flowrate, (C) permeate flux, (D) recovery rate, (E) salt retention, and (F) specific energy.

directly affected the calculated recovery, meanwhile, the other system performance parameters remained comparable at the same *TMP* set-points.

3.1.3. SOWs of BW30 and NF90 membranes with SQFlex 0.6-3 N pump

The SOW is determined by plotting the feed flowrate against the *TMP*. The SOWs of BW30 and NF90 membranes (both with SQFlex 0.6-3 N pump) are shown in Fig. 7A and B, respectively, while the corresponding SOW plots for SQFlex 0.6-2 N pump are provided in Fig. S4. In Fig. 7A, 80% retention was realised at about 5 bar across the set-points (noting the old BW30 membrane could still reach about 92% retention at 12 bar), while the maximum recovery of ~30% was realised within the SOW at 12 bar. This implies that, although a maximum recovery of 30% is desired, this value must occur at least across two to three adjacent set-points (indicated by dashed lines) to form the boundary condition. In the case of the BW30 membrane, a recovery of ~28% was achieved only at the 12-bar set-point, however the maximum recovery that extended across the last three set-points was ~22%, which was therefore used to define the upper boundary. Likewise, the *SEC* and flux values corresponding to the set-points within the SOW were approximately 4 Wh/L and 10 L/m^2.h, respectively.

The SOW with NF90 membrane is shown in Fig. 7B. This is capped by 80% retention and 30% recovery within the membrane's operating range. Due to higher permeability of this membrane, higher fluxes can be realised at higher operating pressure, however operating in these regions would increase the recovery beyond the desired limit. Within the SOW, a *SEC* and flux of 2 Wh/L and ~ 20 L/m^2.h were realised, respectively.

The SOW indicates the possibility of safe operation of the membrane within the investigated *TMP* range, however it does not account for the influence of PV power fluctuations on the pump shutdowns during transient SI conditions, which will be investigated in the next section.

3.2. Determination of resilience thresholds and ROW

The resilience thresholds of ROW were determined through empirical investigation of PV power $\mathscr{D}_{th}$ across different operating *TMPs*: The magnitudes of $\mathscr{D}_{th}$ at which shutdowns occur define the resilience boundary of the ROW (see Fig. 1b).

3.2.1. Resilience test at minimum and maximum operating TMP

Following the method described in Section 2.3.2, sixteen magnitude variations of $\mathscr{D}_{th}$ (ranging from 5 to 80%/s in steps of 5%/s) were simulated and applied to each PV power level (200 W - 550 W). Each $\mathscr{D}_{th}$ magnitude applied lasted for 10 s followed by a recovery period of 10 s before the next magnitude was introduced. The entire sequence of fluctuations lasted ~6 min. The resilience test of SQFlex 0.6-3 N pump with BW30 and NF90 membranes were determined across different *TMP* set-points (5–12 bar). The resilience test results at the minimum (5 bar) and maximum (12 bar) *TMP*s for both membranes are presented in Fig. 8A-D, while the complete test results are presented in the supplementary information Figs. S5 – S8.

The results of BW30 (Fig. 8A and Fig. 8B) highlight two distinct behaviors of pump resilience: First, a direct relation between the pump resilience and operating power: The pump shut down at $\mathscr{D}_{th}$ = 25%/s when the PV power supply was 200 W, reaching a maximum of 75%/s at 550 W. Second, an inverse relation between the pump resilience and the operating *TMP*. At the same power supply of 550 W, the maximum resilience 75%/s was observed at 5 bar, compared to 60%/s at 12 bar under the same conditions.

Likewise, for NF90 membrane as shown in Fig. 8C and D, the two pump behaviors highlighted above applies. The performance difference compared to BW30 however is that NF90 displayed a slightly higher initial resilience at 5 bar set-point: 30%/s vs. 25%/s, suggesting that the higher permeability of the NF90 membrane may enhance pump resilience at lower operating pressures. The power demands of both membranes were comparable with respect to the TMP set-point, indicating that the electrical power characteristic of the pump primarily depends on the operating pressure demand (*TMP* set-point) irrespective of membrane types.

These pump resilience behaviors are explained by the electromechanical characteristics of a helical rotor PDP, following the power-flow process in Fig. 2. At high PV power, the MPPT controller shifts to a higher operating point, increasing array voltage and available current, which raises motor torque and widens the torque reserve relative to the hydraulic load. This allows the motor to tolerate short-term $\mathscr{D}_{th}$ of small magnitude without shutdown, improving resilience. At constant power supply, increasing TMP raises the hydraulic head and torque demand. If the motor cannot meet this demand, pump speed collapses, leading to stalling or shutdown. For example, Grundfos 0.6-2 N and 0.6-3 N pumps automatically cut out below 500 rpm and attempt restart after ~30 s [25,26]. Consequently, high *TMP* operation reduces pump resilience and increases shutdown likelihood

3.2.2. Extended resilience test across all investigated TMP set-points

Extended resilience tests across *TMP* set-points of 5–12 bar and PV

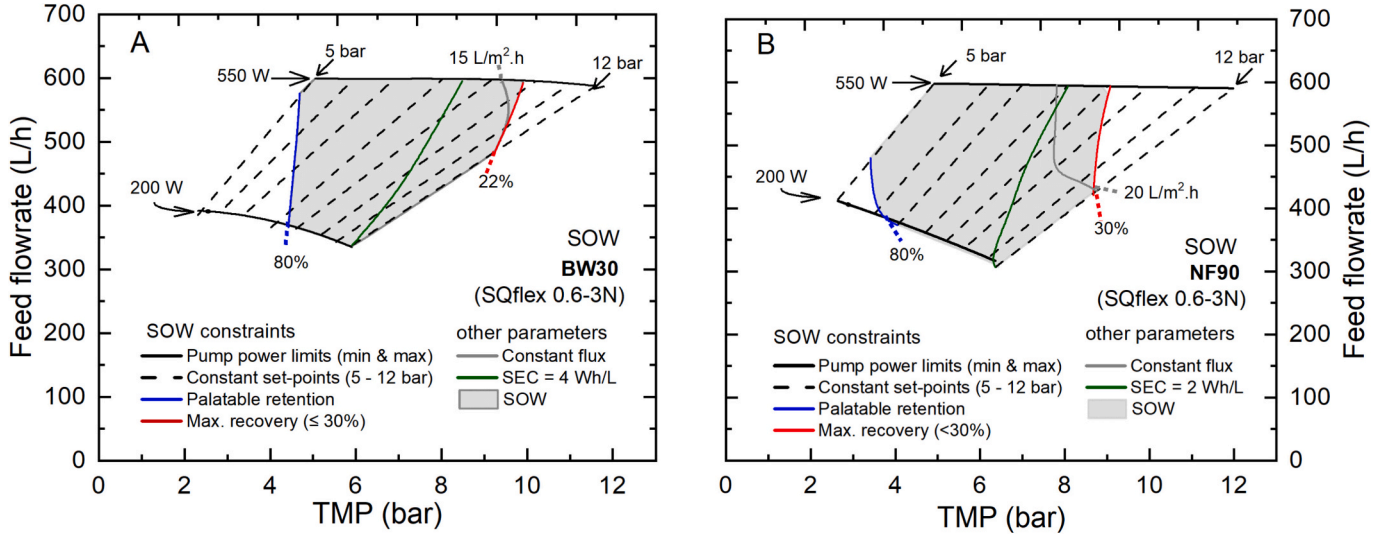

Fig. 7. SOW of PV-membrane system equipped with the SQFlex 0.6-3 N pump, indicating the boundary conditions: Retention ≥80%, tolerable recovery of ≤30%, minimum and maximum power limits, and *TMP* set-points for (A) BW30 membrane, (B) NF90 membrane.

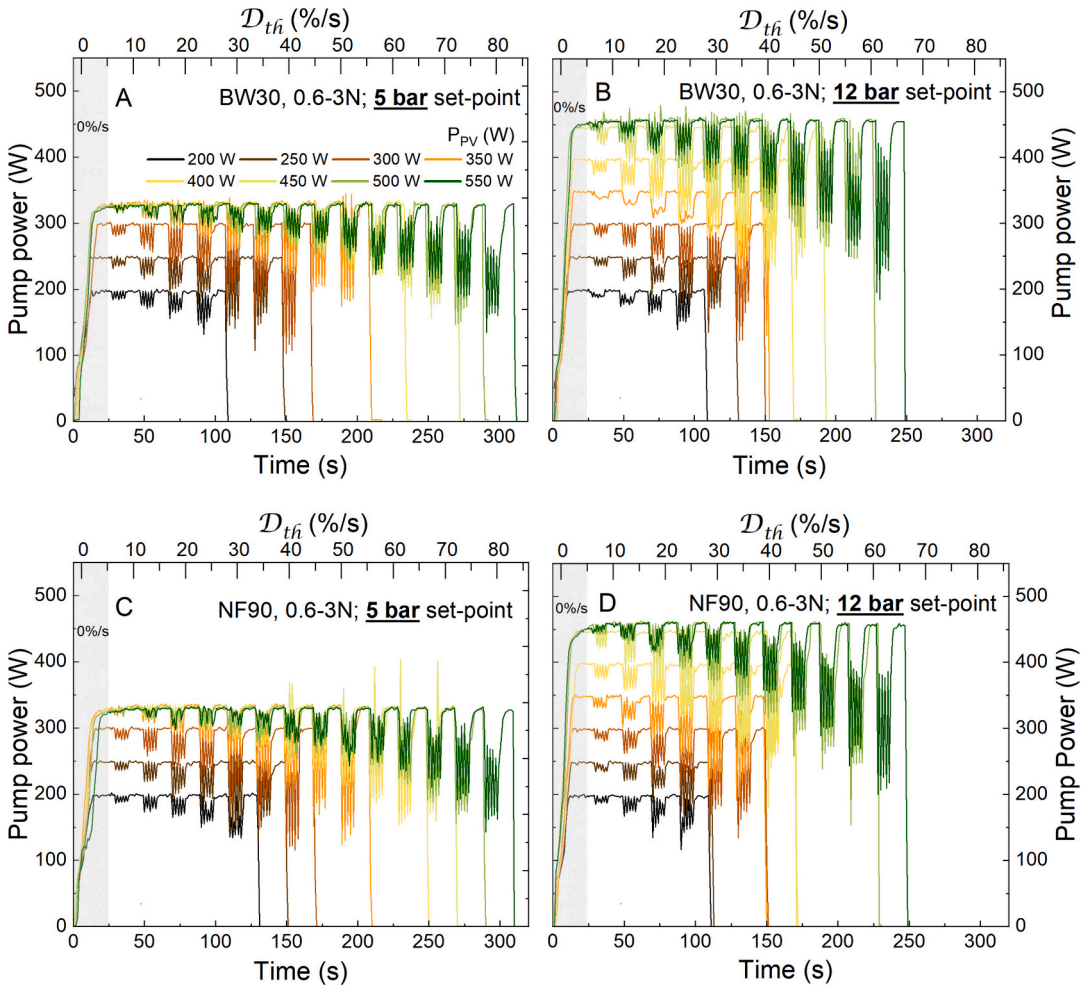

Fig. 8. Shutdown resilience test with SQFlex 0.6-3 N pump, showing $\mathscr{D}_{th}$ = 0%/s – 80%/s investigated for different PV power supply from 200 to 550 W and different membranes and *TMP* set-points. (A) BW30 membrane, 5 bar (B) BW30 membrane, 12 bar, (C) NF90 membrane, 5 bar (D) NF90 membrane, 12 bar.

power levels of 200–550 W for BW30 and NF90 membranes using the SQFlex 0.6-3 N pump are shown as contour maps in Fig. 9A and B, respectively. Corresponding results for the SQFlex 0.6-2 N pump are provided in Fig. S9. The contour plots show the $\mathscr{D}_{th}$ magnitudes at which pump shutdowns occurred, with green indicating high resilience and dark brown low resilience.

For BW30 (Fig. 9A), a minimum shutdown threshold of ~30%/s was observed at 200 W across all pressures. As power increased to 500 W, resilience rose to ~70%/s at 5 bar and decreased to ~55%/s at 12 bar. For NF90 (Fig. 9B), minimum thresholds of 30%/s and 25%/s at 200 W were observed at 5 bar and 12 bar, respectively, indicating reduced resilience at higher *TMP*, more pronounced than for BW30. At 500 W, resilience similarly decreased from ~70%/s to ~55%/s with increasing pressure, consistent with the BW30 results.

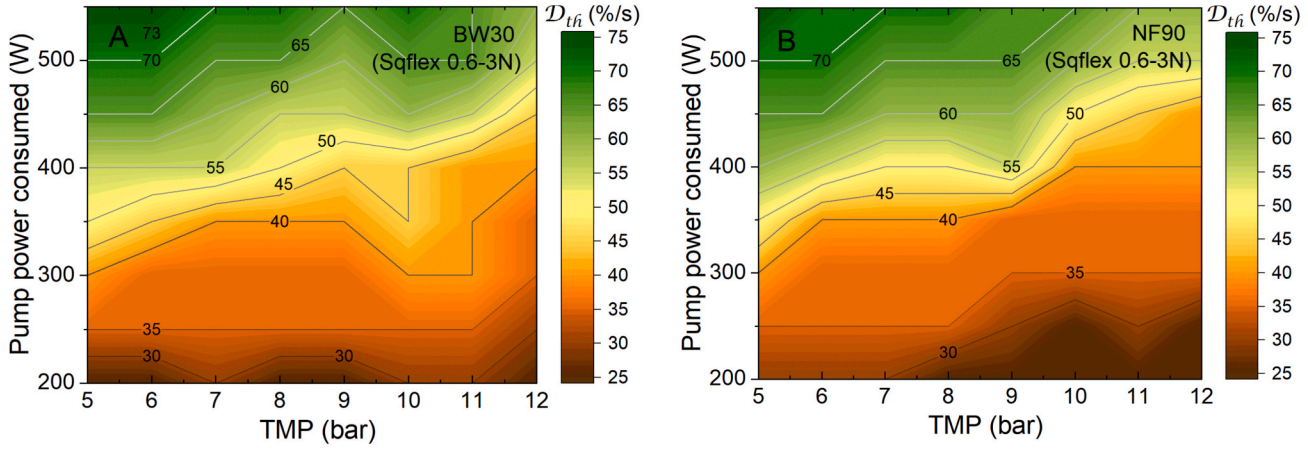

Fig. 9. Contour plots showing the resilience thresholds (quantified in $\mathscr{D}_{th}$, %/s) of PV-membrane pump (SQFlex 0.6-3 N) across different PV power levels (200–550 W) and *TMP* (5–12 bar) for (A) BW30 membrane (B) NF90 membrane.

3.2.3. Transferability of resilience thresholds concept to other PV-membrane systems

The resilience threshold concept can be transferred to other PV-membrane systems empirically by i) defining system-specific critical rates of change in available power beyond which pump shutdowns occur, and ii) expressing these critical values in normalised terms (e.g. %/s of PV power) to determine the $\mathscr{D}_{dt}$ which maps out the resilience boundary. The $\mathscr{D}_{dt}$ are inherently sensitive to system design and component conditions. Pump controller characteristics (e.g. protection logic, sampling frequency) directly influence how power fluctuations are detected and mitigated, thereby affecting the magnitude tolerable $\mathscr{D}_{dt}$ before shutdown. Pump ageing (associated with increased mechanical wear and internal friction), raises start-up torque requirements and reduces hydraulic and electrical efficiency, leading to lower shutdown resilience and reduced tolerable $\mathscr{D}_{dt}$. Conversely, PV array oversizing increases the available power margin and provides additional damping against irradiance fluctuations, enabling larger $\mathscr{D}_{dt}$ values to be accommodated.

As these and various other factors including membrane type, operating TMP set-points, and feed salinity, further contribute to system-specific variations in tolerable $\mathscr{D}_{dt}$, an empirical approach is adopted to identify $\mathscr{D}_{dt}$ under representative operating conditions. Consequently, resilience thresholds should be treated as transferable methodological metrics rather than fixed values, requiring recalibration for each system architecture, component condition, and control strategy.

3.2.4. ROW of BW30 and NF90 membranes

The identified $\mathscr{D}_{dt}$ at minimum power (200 W) in Fig. 8 were used to determine the pump resilience thresholds for the membranes across the *TMP* set-points (5–12 bars). This is summarised in Table 1.

For each *TMP* set-point, the minimum and maximum pump powers were first identified, and their difference was defined as the power magnitude. The empirically determined D_{th} were then applied to this power magnitude to obtain the shutdown power threshold. This was referenced from the lower bound of the SOW to defines the power deviation magnitude from the minimum boundary. The *TMP* and flow that correspond to the power deviation magnitude, traced from the experimental data, were subsequently used to determine the resilience thresholds points. The determined *TMP* and flow data is plotted on the SOW and mapped together to define the resilience threshold of the ROW.

The determined ROWs for BW30 and NF90 with SQFlex 0.6-2 N are presented in Fig. 10. The corresponding ROW results with SQFlex 0.6-2 N pump are provided in Fig. S10.

Within the ROW (shaded region) of BW30 membrane (Fig. 10A), the system can sustain the identified deviations within the pump operating power consumption (200–500 W). Outside the resilience thresholds, the pump is prone to shutdowns. The shutdown is controllable (via back-pressure reduction) during SI fluctuations when the minimum PV power after a ramp down is still sufficient to run the pump ($\geq$ 200 W). Below this power level, the pump is prone to uncontrollable shutdown. For the ROW region of NF90 membrane (Fig. 10B) is similar to BW30 since both membranes are controlled to operate at the same demand *TMP*, albeit NF90 is more loose with higher permeability and lower *TMP* demand to attain the same recovery as BW30. The lower *TMP* demand of NF90 could enhance the pump resilience to shutdown. Due to this, the sensitivity analysis of the ROW with *TMP* variation is subsequently investigated.

3.2.5. Sensitivity analysis of ROW boundary and $\mathscr{D}_{dt}$ with TMP variation

The empirically determined pump power variation curves across different *TMP* set-points were analysed using regression analysis to identify the best-fitting models for each relationship. Since the pump power curves vary exponentially with *TMP*, a nonlinear least-squares fitting method was used to determine the best fits. This was implemented in Excel, with the derived models exhibiting a high degree of agreement with the empirical data, achieving a goodness-of-fit (R^2) $\geq$99% for all *TMP* set-points. The experimental and corresponding fitted model curves, determined for NF90 membrane with SQFlex 0.6-3 N pump, are presented in Fig. S11.

The corresponding models from the analysis were subsequently used to perform sensitivity analysis, quantifying the effect of *TMP* variations on the ROW and its boundaries. This was achieved by first integrating the performance curves in Fig. S11 into a window highlighting the minimum and maximum pump power consumption across all *TMP* set-points, as shown in Fig. 11A. The resulting model curves exhibited a high degree of agreement ($\geq$99%) with the empirical curves, as illustrated in Fig. 11B. Using these model curves, the effects of pressure variations of $\pm$10% *TMP* on the system performance were then investigated.

The need for TMP variation investigation is that most operational changes in PV-membrane systems – such as increases in feed temperature, variations in feed salinity, or changes in membrane permeability due to ageing etc. – directly affect the system's TMP demand.

Table 1
Resilience thresholds identification of BW30 and NF90 membrane with SQFlex 0.6-3 N pump.

Membrane *TMP* Set-point (bar)	Min. pump power (W)	Max. pump power (W)	Power magnitude (W)	Min $\mathscr{D}_{dt}$ (%/s)	Shutdown power threshold (W)	Power deviation Magnitude (W)	Resilience thres.	
							Corr. *TMP* (bar)	Corr. Flow (L/h)
BW30, 0.6-3 N resilience parameters								
5	201	362	161	25	40	241	3.0	439
6	199	380	181	25	45	244	3.7	448
7	199	400	202	30	61	259	4.5	454
8	199	421	222	25	55	255	5.0	424
9	199	438	239	25	60	258	5.8	423
10	200	457	257	30	77	277	6.7	428
11	200	472	272	30	82	282	7.2	417
12	196	485	289	25	72	268	7.4	401
NF90, 0.6-3 N resilience parameters								
5	199	332	133	30	40	239	3.3	470
6	199	351	152	30	46	244	4.3	453
7	199	367	168	30	50	250	5.0	442
8	199	384	185	25	46	245	5.6	421
9	199	405	206	25	51	250	6.2	410
10	199	426	227	25	57	256	6.8	406
11	199	440	241	25	60	260	7.5	392
12	199	461	262	25	65	264	7.8	378

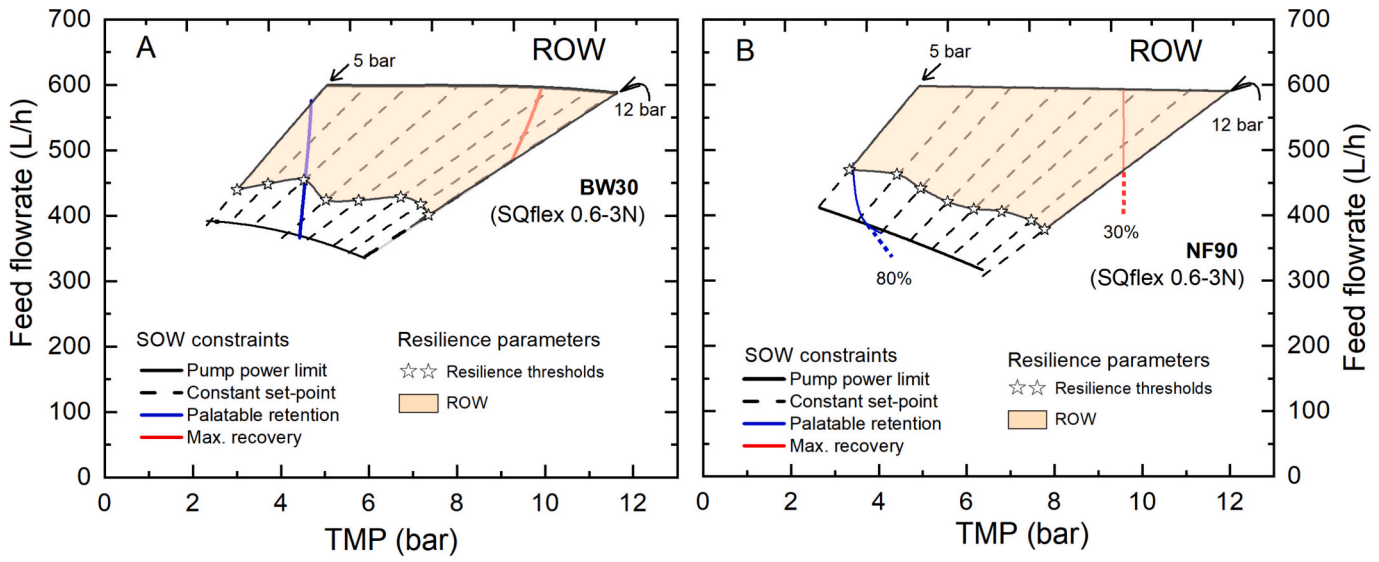

Fig. 10. ROW of PV-membrane system with SQFlex 0.6-3 N pump (A) BW30 membrane, (B) NF90 membrane.

At −10% *TMP* drop, the analysis shows a reduction in pump peak power demand relative to the empirical peak values by ~9% at 5 bar and up to ~16% at 12 bar. This is determined from the data reported in Table S1. Likewise, the deviation sensitivity of the resilience thresholds was reduced from 19% at 5 bar and up to 24% at 12 bar (Fig. 11C). At +10% *TMP* increase, the pump peak power demand increased relative to the empirical values by ~16% at 5 bar and 23% at 12 bar (Fig. 11D). This also shifts the empirical resilience thresholds upward by 22% at 5 bar and 28% at 12 bar. These thresholds and the sensitivity to *TMP* variations are summarised in Table S2.

The boundary shifts in Fig. 11D indicate that an increase in *TMP* in a PV-membrane system (e.g due to increased feed salinity, elevated feed temperature, membrane ageing, fouling, etc) necessitates additional pump power to maintain operation. However, as the resilience thresholds shift upward concurrently, the available resilience margin relative to the reference peak pump power is reduced. In the absence of additional available PV power to meet this increased demand, the system becomes more susceptible to shutdowns, with the likelihood of shutdown increasing as *TMP* demand rises. In contrast, lower *TMP* requirements reduce pump power demand and increase the available resilience margin relative to the peak pump power, thereby enhancing the system's resilience to shutdowns.

The resilience sensitivity analysis presented above was conducted using pump power versus *TMP*, as pump power directly represents the dynamic load experienced by the pump and therefore provides a more sensitive and immediate indicator of conditions leading to pump shutdown. This approach does not invalidate the ROW and R-SOW previously determined from feed flow versus *TMP*, which remains suitable for evaluating membrane performance under steady-state and controlled operating conditions. Also, since pump power is directly proportional to flow, the resilience thresholds from the power-*TMP* curves (as in the case of NF90–0.6-3 N demonstrated here) follow a similar pattern to those obtained from the flow-*TMP* curves.

3.2.6. *Membrane ageing effect on ROW*

Membrane ageing in pressure-driven desalination systems primarily leads to reduced water permeability (or flux) due to compaction or fouling, which manifests as increased TMP demand for a given operating set-point. A sensitivity analysis conducted and shown in Fig. 11 examines the system response to TMP shifts, which indicates that, increased TMP demand, e.g. due ageing, leads to reduced resilience, as reflected by a contraction of the resilience region of the ROW shown in Fig. 11D. This demonstrates that membrane ageing does not alter the shutdown mechanism but shifts the operating point towards higher pump power demand, thereby reducing tolerance to PV power deviations.

3.3. *R-SOW of BW30 and NF90 membranes with high-head positive displacement pump SQFlex 0.6-3 N*

One of the primary objectives of this study is to establish the R-SOW, which, when demonstrated for real-world operation of a PV-membrane system, ensures not only that the system operates within the SOW conditions, but also that it remains resilient (preventing pump shutdowns) during transient PV power fluctuations. The R-SOWs of the BW30 and NF90 membranes operated with the SQFlex 0.6-3 N pump are presented in Fig. 12. These were derived by merging the respective SOWs (Fig. 7) with the corresponding ROWs (Fig. 10) for each membrane. The corresponding R-SOW results obtained with SQFlex 0.6-2 N are presented in Fig. S12.

In Fig. 12A, the R-SOW of the BW30 membrane is bounded by its corresponding SOW conditions. The selection of a 22% recovery for this membrane has been justified in Section 3.1.3. The implication of this R-SOW is that, at system operates of ≥22% and corresponding *TMP* (~10 bar), the permeate quality remains within the acceptable range for drinking water. If the recovery drops below this value, the SOW shifts leftward, leading to reduced permeate quality, which may drop below the desired drinking-water threshold (<80% retention).

In this R-SOW, a rapid power drop ($\mathscr{D}_{dt}$ > 25%/s – which is approximately the same percentage drop in pressure), results in system shutdown like in SOW. However, within the R-SOW region, the system remains resilient to this $\mathscr{D}_{dt}$. To maintain operation within this R-SOW region, a control algorithm is implemented to mitigate the effects of such deviations by promptly reducing the back pressure when the fluctuations approach the identified threshold. The indicated *SEC* of 4 Wh/L is the *SEC* that intersects multiple set-points within the operating window, notwithstanding, if the system is operated specifically at 12 bar set-point, a *SEC* of ~3.5 Wh/L can be achieved as previously shown in Fig. 5 steady-state plot.

The R-SOW determined for the NF90 membrane using the same pump is presented in Fig. 12B. The shaded region, representing the R-SOW, indicated the operating range in which the system remains resilient to ~20%/s deviation threshold. Notably, the *TMP* was reduced to ~8 bar to achieve the target recovery of 30%, as the NF90 is a looser membrane with a higher flux compared to BW30. This lower-pressure operation presents a minor limitation when using the NF90 membrane within the R-SOW, which may warrant further investigation into

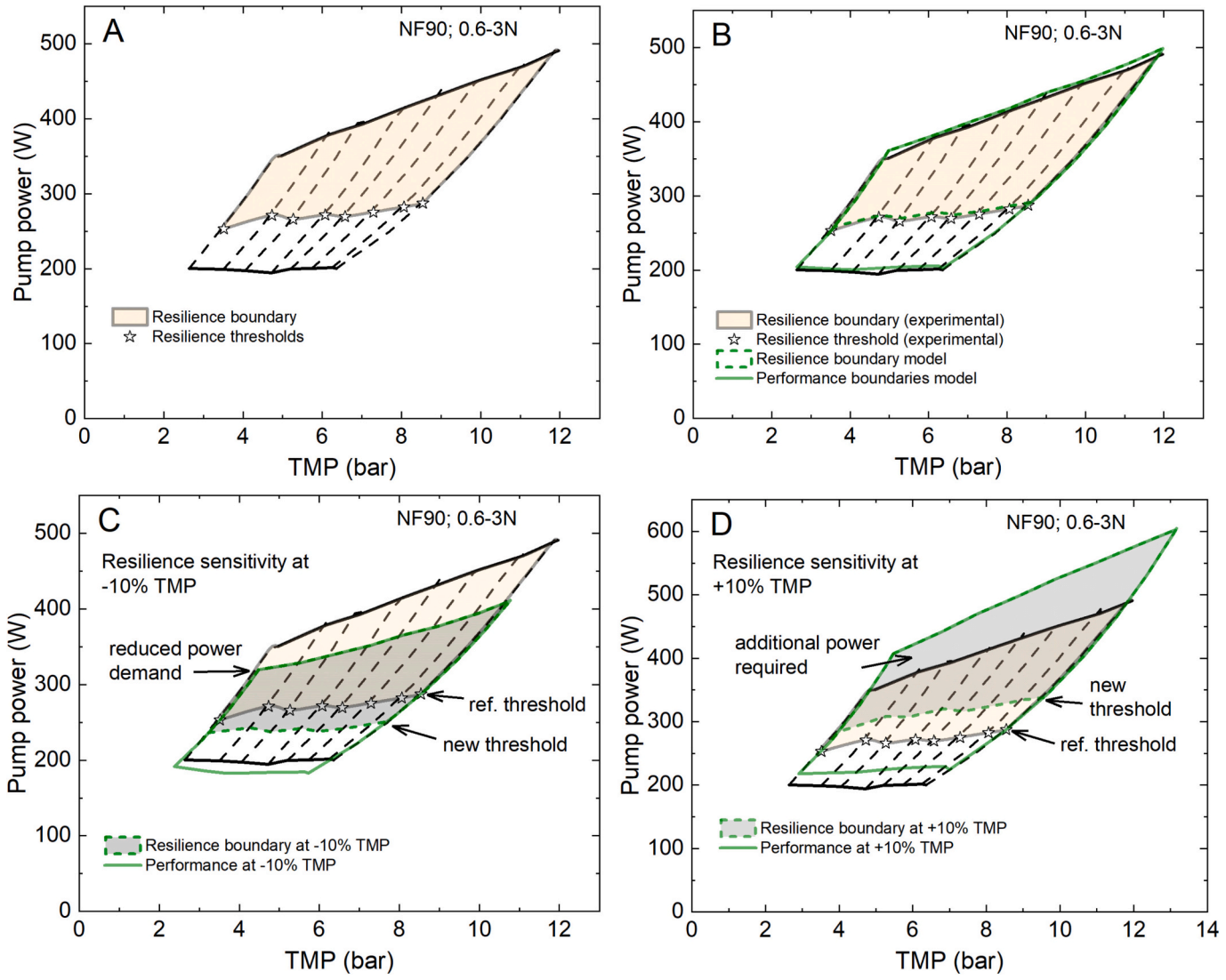

Fig. 11. Pump resilience thresholds based on pump power and membrane operating *TMP* set-points. A. Resilience boundary from empirical testing. B. Comparison of resilience boundary from empirical testing with model boundary. C. Modeled performance analysis at −10% *TMP* variation D.Modeled performance analysis at +10% *TMP* variation.

strategies for minimising production loss once the system reaches its R-SOW threshold. Nevertheless, this membrane-pump combination demonstrated good salt retention (>80%) even at lower *TMP* set-points. The *SEC* of ~2 Wh/L cuts through multiple set-points within the R-SOW, but at 12 bar set-point, it is possible to realise a slightly lower *SEC* of ~1.8 Wh/L as shown previously in Fig. 6 the steady-state plot.

For both figures, the minimum retention (blue) and maximum recovery (red) boundary lines were extended to indicate the possible area of the expected data points when the feed flow rate is plotted against the *TMP* under real-world conditions. In this case, the data points that fall towards the origin of the plot indicate possible shutdowns in the system, as the *TMP* drops to zero when the pump shuts down. Moreover, the unshaded area within these boundaries, below the R-SOW, represents regions where the control algorithm is required for shutdown control, since deviations within the resilience windows do not necessarily lead to system shutdowns.

3.4. Real-world demonstration of PV-membrane R-SOW

A real-world performance evaluation of the PV-membrane system was conducted on a very cloudy day to investigate the system performance when operated within the R-SOW boundary conditions. The very cloudy solar day was selected since it consists of different levels of SI fluctuations which can produce various $\mathscr{D}_{\mathscr{U}}$ relevant to investigate pump resilience to shutdowns under different conditions (operating windows, pump types, and membranes combinations). The performance test within the R-SOW was implemented by setting the maximum recovery of the PV-membrane system to the identified thresholds (i.e., 22% for BW30 and 30% for NF90). The system was then directly-coupled with and powered by the fluctuating PV power supply generated from the partly cloudy day SI data. From the results, the performance region where the permeate retention exceeded 80% was identified and the system behavior was monitored to detect the shutdowns possibility and the number of shutdowns controlled. It was expected that all shutdowns would be mitigated within the R-SOW, except in cases where the available power dropped significantly below the minimum power required for the pump operation (<200 W). System operation under the R-SOW boundary conditions was compared with the corresponding performance under the SOW boundary conditions (without shutdown control), which served as the reference experiment. The results for the BW30 and NF90 membranes operated with the SQFlex 0.6-3 N pump are presented in this section, while the corresponding results for the SQFlex 0.6-2 N pump are provided in Fig. S13 and S14.

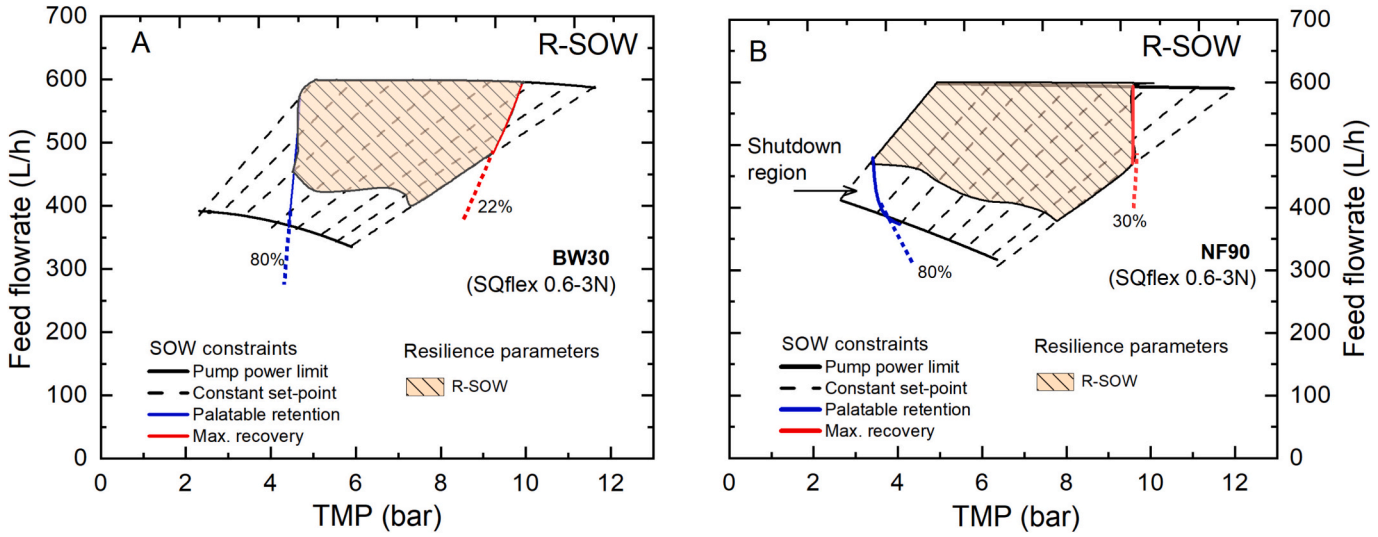

Fig. 12. R-SOW of PV-membrane system with SQFlex 0.6-3 N pump, showing the region of shutdown resilience across different *TMP* set-points within the SOW for (A) BW30 membrane (B) NF90 membrane.

3.4.1. *Performance of BW30 membrane and SQFlex 0.6-3N pump under SOW and R-SOW boundary conditions*

The system performance of BW30 membrane operated with SQFlex 0.6-3 N pump under real-world SI condition is shown in Fig. 14. Fig. 14 A-E gives the results of operation under SOW boundary conditions, while Fig. 14 F-J shows the system performance under R-SOW boundary conditions. In Fig. 13A, nine pump shutdowns were observed which also correspond to the same number of shutdowns on the *TMP*. The *TMP* peaked at ~11 bar (Fig. 13B) in line with the maximum operating pressure within the R-SOW boundary conditions. Within the same operating condition, a maximum permeate flow rate of about 125 L/h was realised (Fig. 13C). This indicates a recovery of about 22% (similar to the SOW plot in Section 3.1.3, Fig. 6), since the maximum flow rate of this membrane is approximately 580 L/h at a *TMP* of ~12 bar. Additionally, the permeate EC (Fig. 13D) recorded an average of approximately 0.7 mS/cm, which shows that the production is within the SOW for drinking water ($\leq$ 1.1 mS/cm $\approx$ 1 g/L TDS). A maximum rejection of about 90% and recovery of 22% were observed (Fig. 13E), except for occasional spikes during system shutdowns during system shutdowns.

The implementation of the shutdown control algorithm within the SOW boundary conditions to realise an R-SOW shows, firstly ~67% reduction in shutdowns from nine to three (Fig. 13F). The uncontrollable shutdowns were observed to occur when the power dropped below the pump's resilient limit, thus resulting in unavoidable shutdowns. This led to an equal number of shutdowns in the *TMP* (Fig. 13G). Although a permeate flow rate of about 125 L/h was realised (Fig. 13H), giving a similar recovery of ~22% as under the SOW condition, the cumulative daily production within the SOW conditions increased by 8 L (524 L vs 518 L). This could be attributed to the reduced number of shutdowns. Nevertheless, the average permeate EC realised within the R-SOW (Fig. 13I) was comparable to that of the SOW (Fig. 11D) at about 0.7 mS/cm. Likewise, maximum rejection and recovery of about 90% and 22% were realised (Fig. 13J) during the transient operation. For both performance results (SOW and R-SOW), a comparable minimum *SEC* of ~4.0 Wh/L was realised.

A closer examination of the unavoidable shutdowns shown in Fig. 14F, indicating the sub-resilient PV power level is shown on Fig. 14. Fig. 14A-C show respectively the three identified shutdowns under the R-SOW conditions. For each plot, the transient open circuit maximum PV power (black line), PV power supply on load (red line), and power consumed by the pump (blue line) are presented over the time axis of seconds. In Fig. 14A, the maximum PV power initially at ~470 W had a sharp ramp down to ~200 W within 7 s. In the first second, the power consumed by the pump (blue) experienced a ramp down (~450 W to ~360 W) with $\mathscr{D}_{dt}$ = 20%/s. This threshold was not expected to cause the pump shutdown; however, the shutdown became inevitable when the maximum PV power supply (black) dropped to ~150 W. The rate of PV power rampdown in the second shutdown event of Fig. 14B, starting from ~325 W, had less drastic effect at about $\mathscr{D}_{dt}$ = 10%/s. This should likewise not result in the pump shutdowns, but the shutdown later occurred when the maximum PV power dropped to ~150 W. In the third shutdown event of Fig. 14C, the pump power consumption dropped from ~360 W to ~250 W in the first drastic ramp down event resulting in $\mathscr{D}_{dt}$ = ~30%/s. This threshold is expected to trigger an immediate shutdown of the pump. Moreover, the concurrent drop in PV power to ~150 W (below the pump's minimum resilience threshold) prevented the control system from averting the shutdown. In all three cases, pump shutdowns became unavoidable when the PV power level dropped below 200 W. Although experimental observations indicated a critical shutdown threshold around 150 W, a conservative minimum level of 200 W was defined as the risk threshold – below which any further decrease in power would likely result in an unavoidable system shutdown.

3.4.2. *Performance of NF90 membrane and SQFlex 0.6-3 N pump under SOW and R-SOW boundary conditions*

The system performance using NF90 with the same pump (SQFlex 0.6-3 N), investigated under the boundary conditions (that is, operation at the set recovery and pressure) of SOW and R-SOW, are reported in Fig. 15. Owing to the high recovery characteristics of the NF90 membrane, the system *TMP* was reduced to ~9 bar to realise a recovery of 30%. The first observation was the reduction in shutdowns to two without implementing a shutdown control strategy (Fig. 15A). This is possible because the system now operated at a reduced operating *TMP* of ~9 bar (Fig. 15B) compared to ~11 bar with BW30 membrane: As shown in ROW Fig. 8, reducing the operating pressure lowers the shutdown possibilities. The system operated at a set maximum permeate flowrate of ~150 L/h (Fig. 15C) to realise a maximum recovery of 30% from ~600 L/h maximum feed flow. This resulted in the daily production of 782 L. This system produced an average daily permeate EC of 0.63 mS/cm (Fig. 15D), and about 95% rejection (Fig. 15E) at the same recovery.

Within R-SOW conditions, the implementation of the shutdown control algorithm completely eliminated the shutdowns in the system (Fig. 15F), with comparable effects observed on *TMP* (Fig. 15G). This operation moreover yielded an increase in daily production by ~9 L

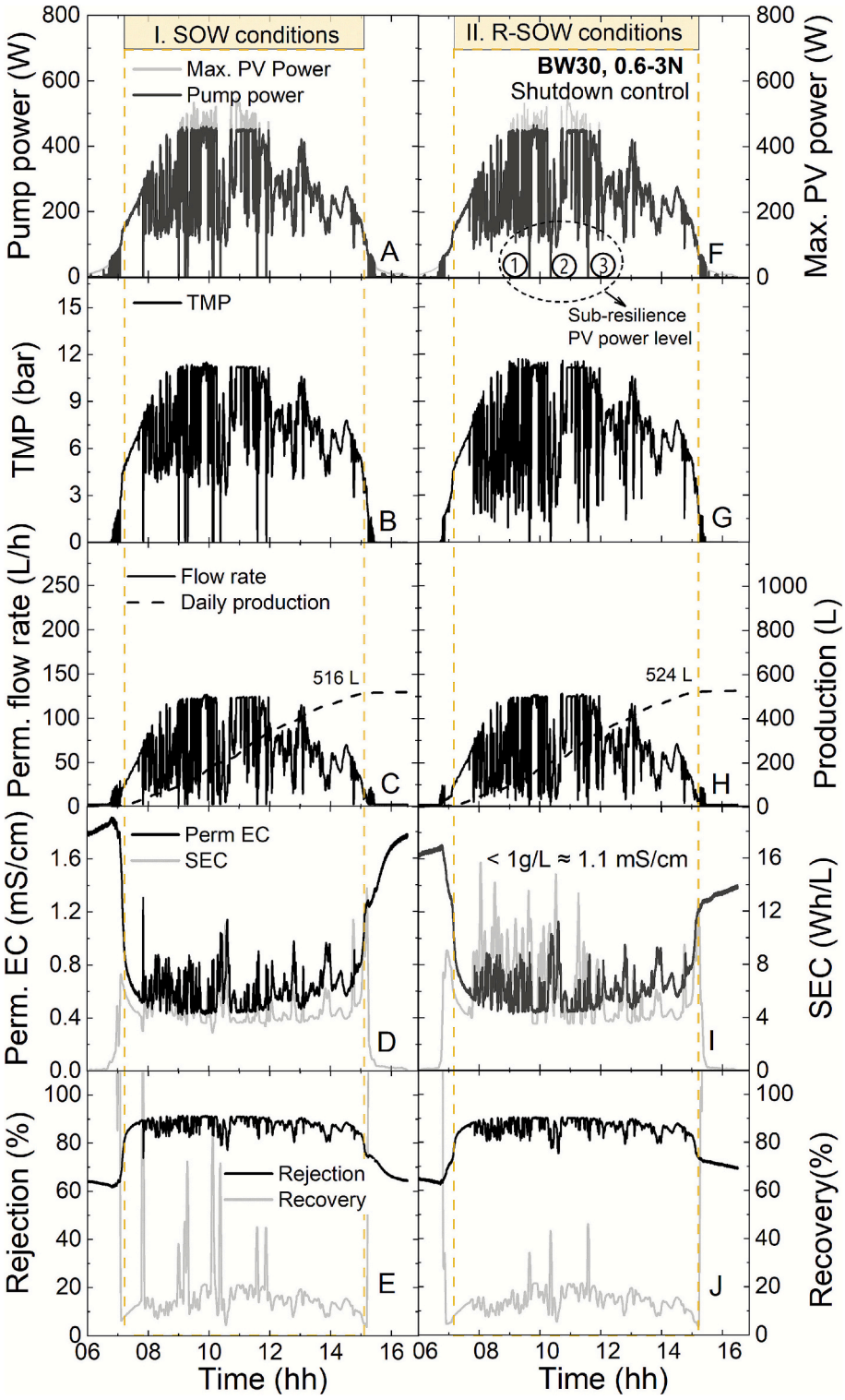

Fig. 13. Performance of PV-membrane system under SOW and R-SOW conditions using **BW30 membrane** and **SQFlex 0.6-3N** pump: (A, F) PV power supply and pump power consumption, (B, G) *TMP*, (C, H) permeate flow rate and cumulative daily production, (D, I) permeate EC and SEC, (E, J) salt rejection and system recovery.

(Fig. 15H) compared to the operation with no shutdown control within SOW boundary conditions, even though both have a capped permeate flow rate of ~160 L/h (≈27% recovery from ~600 L/h maximum feed flow rate). This system has an average EC of ~0.5 mS/cm (Fig. 15I) – a slight improvement to the uncontrolled operation within the SOW conditions – and about 95% rejection was realised with this configuration (Fig. 15J) at the same recovery.

For both performance results (SOW and R-SOW), i) a comparable minimum *SEC* of ~2.3 Wh/L was realised, and ii) the plotted recovery displayed some spikes above the 30% thresholds. These observed spikes in the calculated recovery could be attributed to the dynamic response of the membrane under transient flow conditions [41]. During a rapid drop in feed flow to the membrane, the permeate response is not instantaneous; the permeate flow persists briefly due to water already present

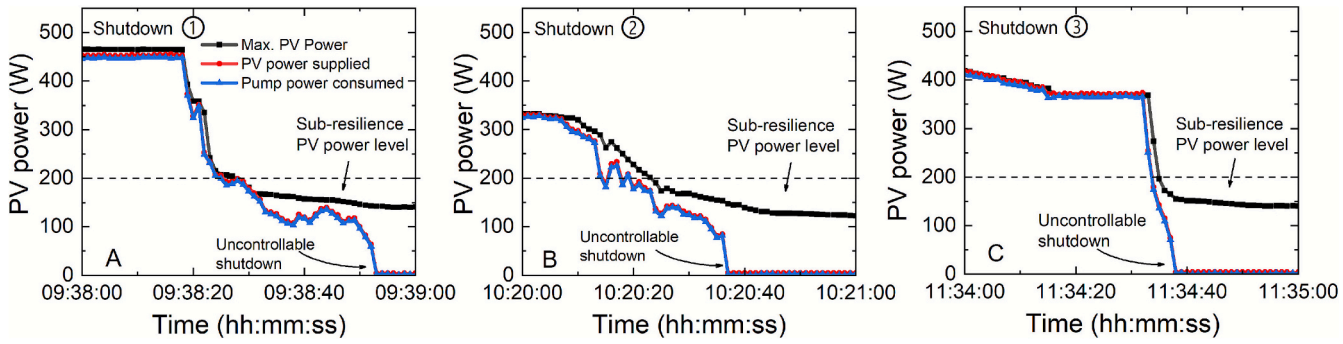

Fig. 14. Shutdowns at sub-resilient PV-power level under R-SOW operating conditions: A. Shutdown ① B. Shutdown ②, C. Shutdown ③.

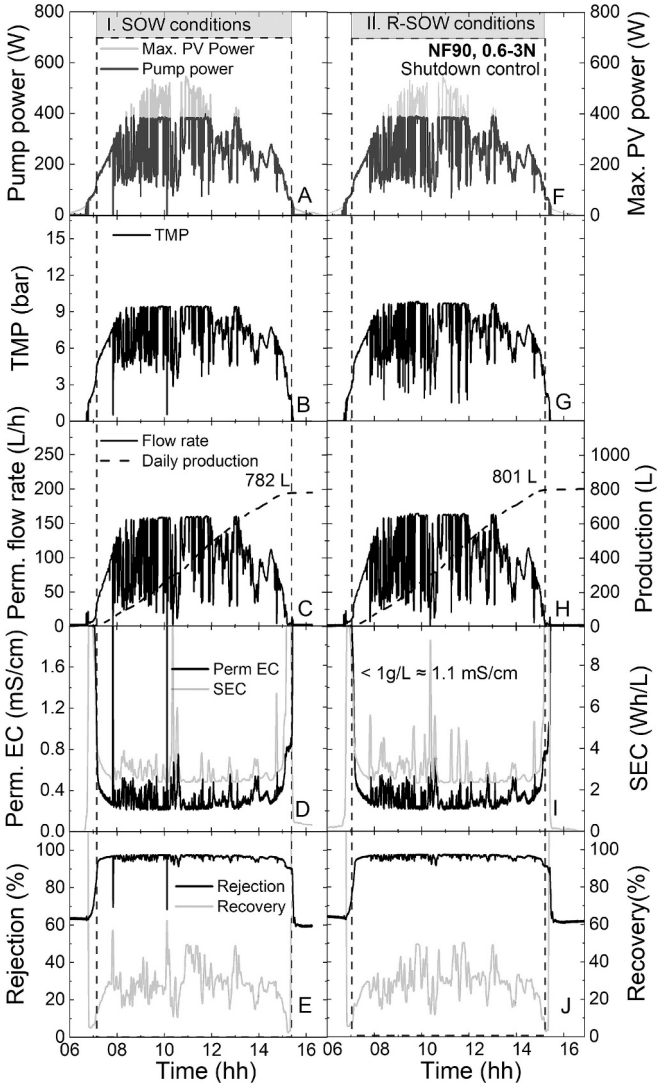

Fig. 15. Performance of PV-membrane system under SOW and R-SOW conditions using **NF90 membrane** and **SQFlex 0.6-3N** pump: (A, F) PV power supply and pump power consumption, (B, G) *TMP*, (C, H) permeate flow rate and cumulative daily production, (D, I) permeate EC and SEC (E, J) salt rejection and system recovery.

within the membrane pores, thus recovery, defined as the ratio of permeate to feed flow often picks some spikes in the process. Thus, the permeate flowrate threshold is observed to give a better indication of recovery in these results.

The summary of the system performance with both membranes and pump operating within the SOW and R-SOW limits are summarised in Table 2, while the corresponding summary table of SQFlex 0.6-2 N pump is given in the Supplementary Information Table S3. The results show that PV-membrane system operation within the R-SOW reduces the number of occurrences of pump shutdowns in the system. This is often associated with an increase in daily production. For BW30 membrane, the system shows ~67% resilience to shutdown (by eliminating 6/9 shutdowns with additional production gain of ~8 L. The remaining shutdowns which were not controlled with BW30 were due to the PV power supply drop below the minimum demand of the pump at ~150 W. The NF90 membrane however enabled100% resilience to shutdown with a production gain of ~19 L compared to the SOW operation. Aside the shutdown controls, operation within the R-SOW control conditions ensures that all system performance are maintained within the desired target of safe operation, especially, <30% recovery and drinkable permeate (<1 g/L ≈ 1.11 mS/cm EC).

An additional investigation using another day (a partly cloudy day) was conducted using NF90 membrane and 0.6-3 N pump. This however resulted in no shutdowns under a directly-coupled SOW condition, therefore no shutdown control and production gain under the corresponding R-SOW condition where the back-pressure was controlled. The result is thus included in the Supplementary Information Fig. S15.

3.4.3. System performance within the operating windows, limitation and recommendation

The experimental data points of feed flow rate and corresponding *TMP* obtained under a very cloudy solar day for both SOW and R-SOW operations with BW30 and NF90 membranes using 0.6-3 N pump are shown in Fig. 16. The corresponding result for 0.6-2 N is provided in Fig. S16. The experimental data points were overlaid on their respective operating windows to illustrate the system's performance within the defined boundaries of each window. About 27,145 and 29,634 data points are located within the SOW and R-SOW of BW30 respectively, indicating that the system operated for ~30 min longer within the R-SOW compared to the SOW. For NF90, the data points within the respective windows are 22,763 and 25,555, with the system operating ~45 min longer in the R-SOW. Also, there are some scattered data points that extended to more areas within the overlapping SOW in the R-SOW. This was due to the back-pressure control implemented within the R-SOW to prevent shutdowns.

The significance of Fig. 16A-D is that they provide insight into i) membrane performance utilisation and ii) possible shutdowns. From the results, BW30 membrane/0.6–3 N pump is more suitable for the system in terms of membrane utilisation. The membrane is utilised when the performance fits into operating set-point within the SOW; however, it can still be prone to shutdowns, which can be mitigated through control within the R-SOW as shown in Fig. 16A and B. The area below the R-SOW but within the SOW represents regions where a control algorithm is required to manage shutdowns. The BW30 membrane system was constrained by ~11 bar *TMP* under both SOW (Fig. 16A) and R-SOW

Table 2
System performance summary under SOW and R-SOW operating conditions.

Pump	Operating window	Membrane	Operating *TMP* (bar)	#Shutdowns (SOW ref)	#Shutdowns eliminated	Daily prod. (L)	Prod. gain (SOW ref) (L)
SQFlex 0.6-3 N	SOW	BW30	~11	9	–	516	–
		NF90	9	2	–	782	–
	R-SOW	BW30	~11	3	6	524	8
		NF90	9	–	2	801	19

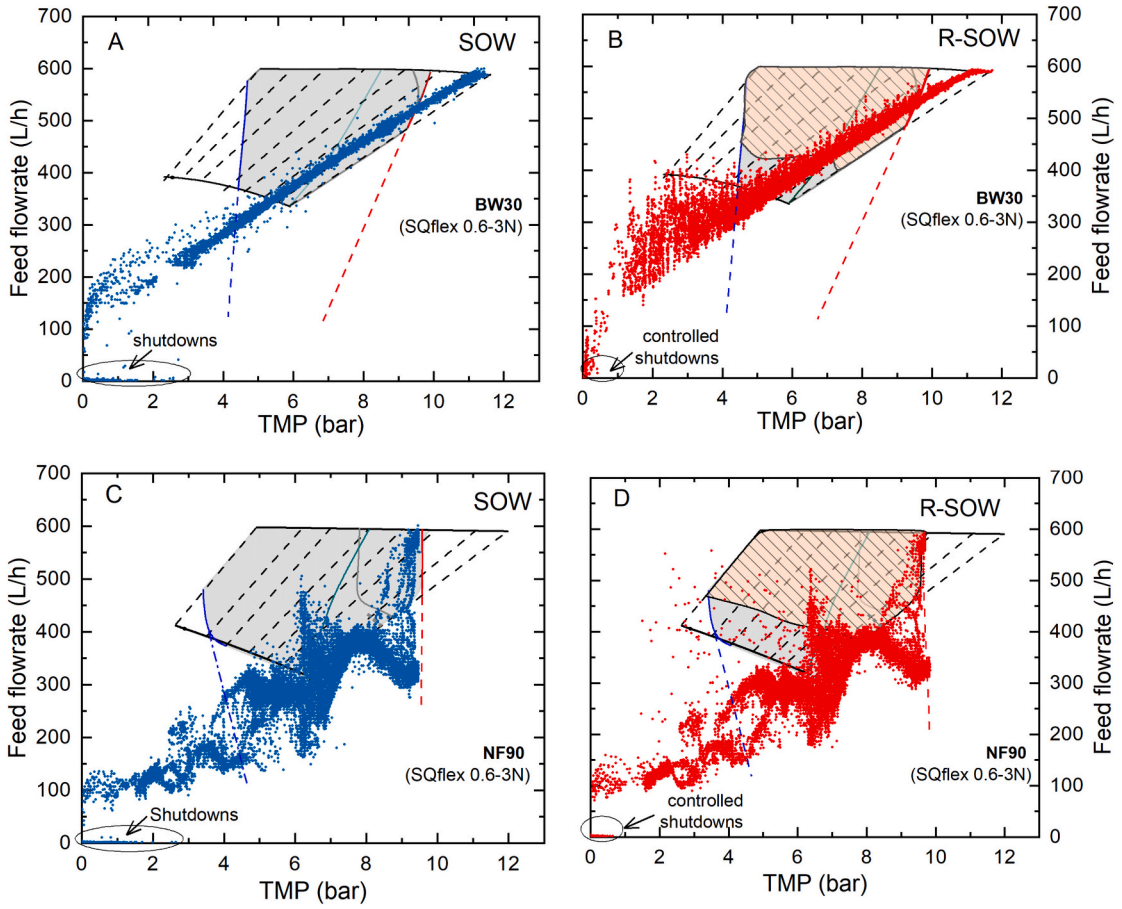

Fig. 16. PV-membrane system performance within the operating windows, showing transient operation data points (blue = SOW, red = R-SOW) of a very cloudy solar day experiments for different membranes using SQFlex 0.6-3 N pump. A. BW30, SOW. B. BW30, R-SOW C. NF90, SOW, D. NF90 R-SOW. (For interpretation of the references to colour in this figure legend, the reader is referred to the web version of this article.)

(Fig. 16B) conditions, since the membrane recovery at this set-point was below the 30% limit. In contrast, the NF90 membrane (Fig. 16C and D) was limited by the 30% recovery threshold under both SOW (Fig. 16C) and R-SOW (Fig. 16D) conditions, due to its higher flux property. Although the NF90 membrane can achieve higher production, operating at high recoveries increases salt concentration near the membrane surface, which can lead to scaling and fouling. The 30% recovery constraint in this study meanwhile helped to reduce shutdown susceptibility under transient PV conditions, since operating beyond this limit would require higher *TMP* demand, which could increase the shutdown chances.

To address the production limitation of the NF90 membrane, especially under high PV power supply, future work could explore adaptive energy recovery control strategies with SI predictive control to dynamically store the excess PV energy when the system recovery is constrained, especially during the peak period of SI. The excess energy can be stored either electrically or hydraulically.

3.5. *Further Investigations with low-head positive displacement pump*

In this section, i) a "very cloudy day" in the prior investigation of NF90 membrane was first repeated with another pump (0.6-2 N) to demonstrate the shutdown control with another configuration, and ii) three additional solar days were investigated using the same pump to check the effect of different irradiance data on the same configuration. The 0.6-3 N pump was not selected for the extended operation because it operates at approximately 50% of its maximum head capacity (~10 bar set-point compared to 20 bar maximum head capacity) under the low SOW recovery conditions (30%) considered in this study. This provides a larger hydraulic and torque margin, making the pump more resilient during high PV power supply, thus requiring higher PV power D_{th} to trigger a shutdown. The three additional solar days were taken from the SI and temperature data from KIT Solar Park: **Day 1**: A partly cloudy day (5th may 2016), **Day 2** (20th June 2016) and **Day 3** (24th June 2024). All experiments were conducted under both SOW and R-SOW conditions, and the results are presented in this section.

Using this pump-membrane configuration (0.6-2N, NF90), under the

SOW recovery of 30%, five shutdowns were observed in pump power supply (Fig. 17 A) and *TMP* (Fig. 17 B). This resulted in daily production of 789 L (Fig. 17 C). The average permeate EC was ~0.6 mS/cm (Fig. 17 D) and the permeate quality was drinkable at ~95% retention (Fig. 17 E). The complementary investigation under R-SOW condition where the back-pressure control was implemented to mitigate the pump shutdowns, shows that all shutdowns were prevented in pump power (Fig. 17 F) and *TMP* (Fig. 17 G). There was a daily production of 794 L yielding an additional 5 L gain. Likewise, the permeate quality remained within a drinkable limit at ~0.5 mS/cm (Fig. 17 I) with rejection of about 95% (Fig. 17 J).

3.6. Extended operation across multiple solar days with positive displacement pump

Additional solar days experiments of the was conducted using another PDP (a low-head 0.6-2 N) under the SOW condition of 30% recovery. On Day 1, the pump power consumption was ~380 W (Fig. 18 A) with a corresponding *TMP* of ~10 bar (Fig. 18 B). This configuration

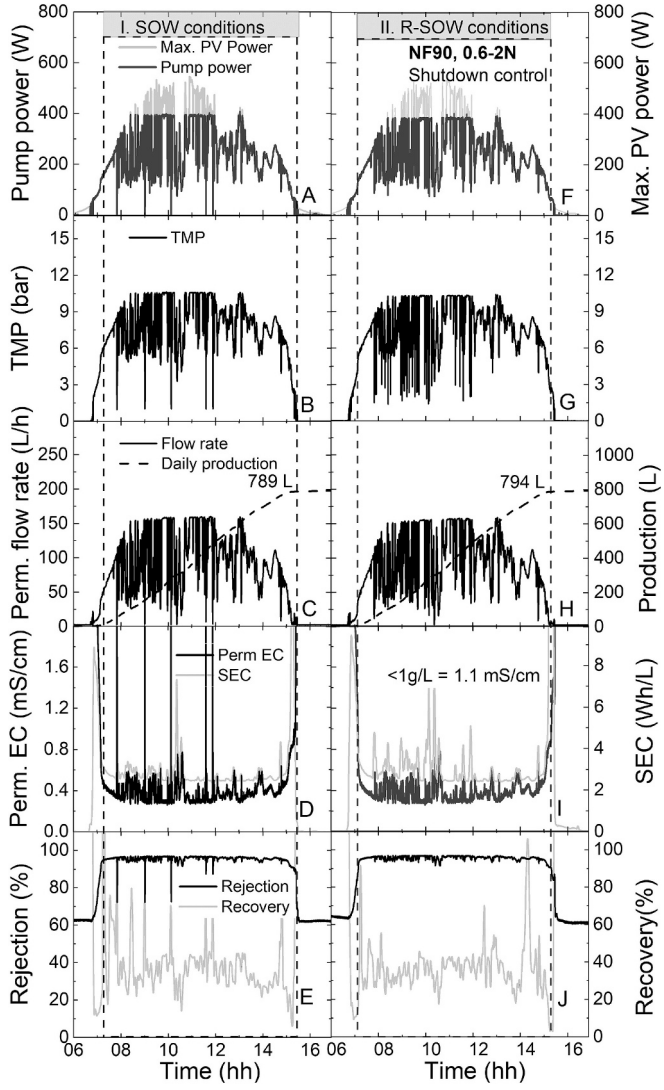

Fig. 17. Resilient operation of **NF90** membrane and **SQFlex 0.6-2N** pump under highly fluctuating solar irradiance (cloudy day). Column I: Passive (directly-coupled) operation as reference; Column II: R-SOW operation with shutdown control. (A, F) PV power supply and pump power consumption, (B, G) *TMP*, (C, H) permeate flow rate and cumulative daily production, (D, I) permeate *EC* and *SEC*, (E, J) salt rejection and system recovery.

resulted in no shutdowns, with a daily yield of ~1254 L (Fig. 18 C). On Day 2, under the same recovery and power condition, there was an overlapping of about 3 shutdowns at the middle of the day (Fig. 18 D) with corresponding shutdowns in *TMP* (Fig. 18 E), producing the total daily yield of 1171 L (Fig. 18 F). Day 3 was characterised by multiple fluctuations with about eight shutdowns of pump power (Fig. 18 G) and *TMP* (Fig. 18 H) during the day, with a cumulative daily production of 1356 L.

These days were repeatedly investigated under the R-SOW condition where the back-pressure control was implemented to mitigate the shutdowns at the dame recovery threshold of 30%.

The results as shown in Fig. 18 for Day 1 shows no addition shutdown on pump power (Fig. 19 A) and *TMP* (Fig. 19 B), with about the same daily production of ~1254 L. On Day 2, about 2 shutdowns were prevented in the middle of the day for the pump power (Fig. 19 D) and *TMP* (Fig. 19 E), with daily production of 1175 L, a slight gain of 4 L, compared to the directly-coupled configuration. On Day 3, the previously 8 shutdowns were reduced to two shutdowns in pump power (Fig. 19 G) and *TMP* (Fig. 19 H). This resulted in daily production of 1364 L, which is an 8 L gain compared to the uncontrolled directly-coupled configuration.

3.7. Transferability of resilience framework to PV-powered pumps

Although this study experimentally demonstrates pump resilience operation using two helical rotor PDPs from Grundfos, the framework is a system-level concept that captures the interaction between i) PV power variability, ii) motor-drive shutdown thresholds (based on the electro-mechanical limits and internal control logic), and iii) hydraulic load characteristics (variability of pressure demand). As such, the resilience concept can be transferred to other PV powered PDP designed for high pressure operation such as water pumping system or membrane desalination application.

3.7.1. The generality of resilience concept for PDPs

For all PDPs, the required shaft torque scales approximately linearly with discharge pressure, and weakly dependent on rotational speed [16]. Consequently, shutdown resilience is strongly pressure-dependent, and operation at higher set-points (albeit enables the pump to operate at its best performance efficiency) however reduces the available torque margin (during PV power fluctuations), leading to lower tolerance to rapid PV power deviations. In contrast, centrifugal pumps exhibit fundamentally different hydraulic behavior, with torque and power demand approximately proportional to the square and cube of rotational speed, respectively [17]. At reduced speeds, centrifugal pumps have a lower torque demand on the motor. This can provide greater tolerance to short-term power drops and broader resilience region at low pressure. Meanwhile, for small scale membrane desalination unit where low flow is required at high pressure, PDPs are mostly preferred and utilised in applications [37,42–44]. Thus, irrespective of the PDP type or motor drive, the pump shutdown occurs when the available electromagnetic torque is no longer sufficient to balance the instantaneous hydraulic load torque. For transferability of this concept, the resilience pump limit can first be determined empirically, following the procedure described in Section 2.3.2. This threshold is then implemented to control the shutdown during PV power fluctuations.

3.7.2. Common shutdown indicators from performance curve for PDPs

All pumps have performance curve, with PDPs generally showing the relationship between the flow rate, and power (sometimes including pump efficiency) for a given pump head (pressure). The performance curves of two helical rotor submersible PDP used in this study: SQFlex 0.6-2 N and 0.6-3 N are shown in Fig. 20A and B respectively. The key highlight of these curves is that the Pump "shut-off" power. When the power supply falls below this threshold, the electromagnetic torque becomes insufficient to overcome the hydraulic load and the pump

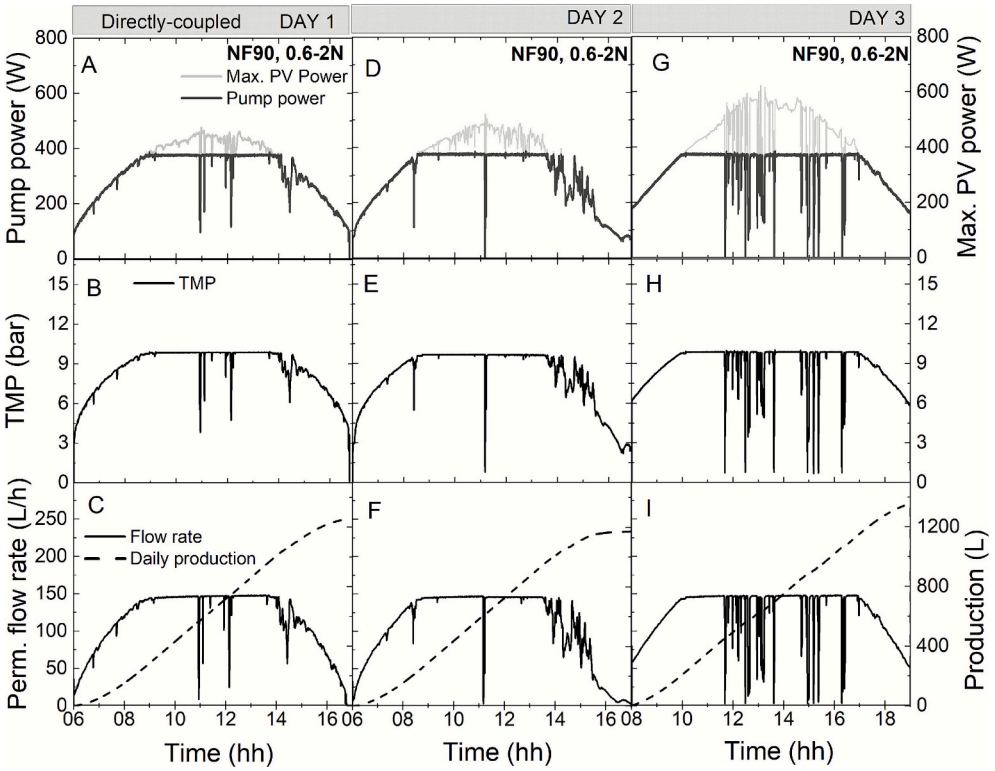

Fig. 18. Multiple days operation of **NF90** membrane with **low-head pump** SQFlex **0.6-2N** under a **directly-coupled (SOW) condition.** *Day 1*: multiple ramp downs with no pump power shutdown; *Day 2*: mostly clear day with about three overlapping shutdowns at the middle of the day; *Day 3:* another partly cloudy day with seven shutdowns. (A,D,G) PV power supply and pump power consumption, (B,G,H) *TMP*, (C,F,I)) permeate flow rate and cumulative daily production.

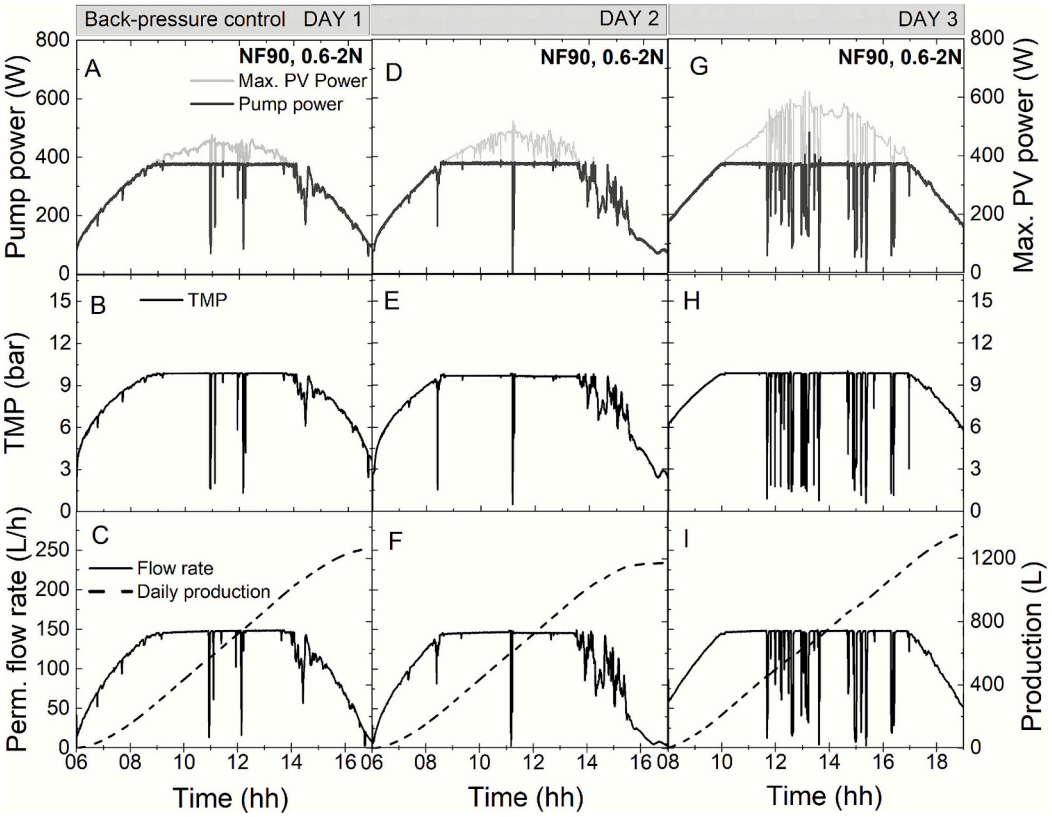

Fig. 19. Multiple days operation of **NF90** membrane with **low-head pump** SQFlex **0.6-2N** under a back-pressure control (R-SOW) condition. *Day 1*: multiple ramp downs with no pump power shutdown; *Day 2*: mostly clear day with about three overlapping shutdowns at the middle of the day; *Day 3:* another partly cloudy day with seven shutdowns. (A,D,G) PV power supply and pump power consumption, (B,G,H) *TMP*, (C,F,I)) permeate flow rate and cumulative daily production

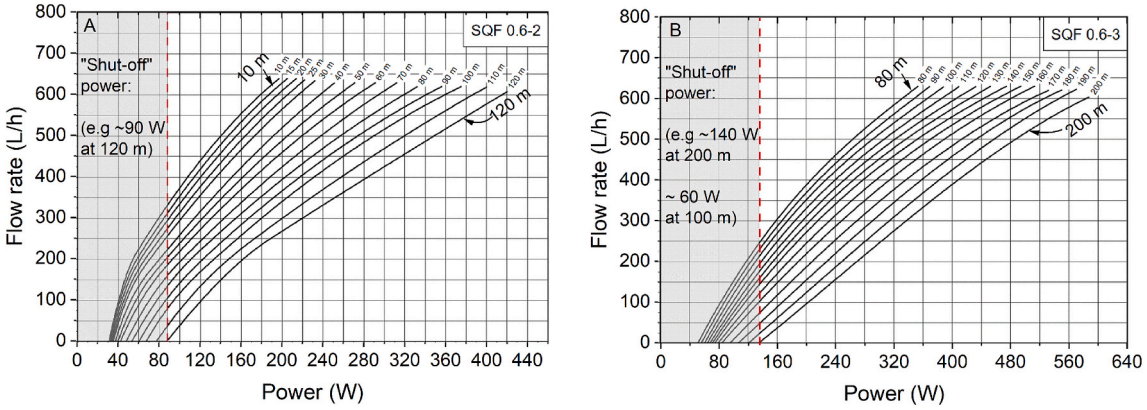

Fig. 20. Performance curves of two Grundfos helical rotor positive displacement pumps: A. model 0.6-2 N [25]: B. model 0.6-3 N [25,26].

reaches a stalling condition – where the motor continues to work against pressure, but the pump no longer produces measurable flow. To avoid this, the pump control triggers a protective shutdown.

The shut-off power increases with operating head (or pressure demand). For example, the shut-off power for low-head pump 0.6-2 N increases from ~30 W at 10 m to ~90 W at 120 m (Fig. 20A), and from ~55 W at 80 m to ~140 W at 200 m for high-head pump 0.6-3 N (Fig. 20 B). These "shut-off" power represents ~**21% (0.6-2 N)** and ~**24% (0.6-3 N)** of each pump's rated maximum power of 420 W and 590 W respectively. A control margin above these limits, e.g. up to 30% of the maximum power at each operating head can be recommended at the minimum threshold to prevent the pump from stalling. This shut-off shutdown limit is common to most pumps, and the thresholds can be determined from the pump's performance curves.

Shutdowns through PV power deviations do not occur as a single abrupt event. Cloud edges are spatially diffuse and temporally dynamic, causing PV power to ramp down in multiple steps rather than as a single instantaneous drop. Consequently, as PV power decreases gradually, while the membrane *TMP* also reduces proportionally in a stepwise manner. The slow startup is also maintained via the pump CCU each time the pump shuts down. These respectively help to prevent rapid depressurisation or pressurisation of the membrane in PV-membrane system. Frequent shutdowns have also been reported not to affect membrane integrity [45], making PV-membrane system still dependable. Although the initial power deviation (e.g., ~30%/s) may not necessarily lead to pump shutdown if the operating point remains sufficiently above the shut-off power, it is an indication that shutdown can be imminent if not controlled immediately.

4. Conclusion

Previous studies have investigated the SOW to identify regions of optimal membrane performance under steady-state conditions, typically constrained by parameters such as a maximum recovery of 30%. However, these analyses were based on constant power supply and did not account for real-world transient conditions, where frequent PV power fluctuations can trigger repeated shutdowns, reduce the system performance (e.g. daily water production and permeate quality) and increase the specific energy consumption (*SEC*).

In this study, two significant operating windows of a PV-membrane system under transient operation are defined: the ROW and the R-SOW. The ROW defines the region where the system can be resilient to shutdowns across multiple pressure set-points, while the R-SOW (a merger of the ROW and SOW) represents the region where the system remains both resilient to power fluctuations and while maintaining optimal membrane operating limits, thus providing a more realistic framework for assessing real-world PV-membrane system performance.

These are defined through empirically identified PV power deviation thresholds ($\mathscr{D}_{\mathscr{M}}$) that trigger pump shutdowns for different pump-membrane configurations across a range of transmembrane pressure (*TMP*) demands. Although, based on empirical testing, the $\mathscr{D}_{\mathscr{M}}$ which define the ROW may be pump-specific, since they can depend on factors such as the pump's internal control logic, maximum pump head, and the operating load (in this case, the membrane *TMP* set-point), the underlying concept of pump shutdowns can however be transferable to other similar pumps used for PV-powered membrane desalination system.

The R-SOW was experimentally investigated for two membranes (BW30 and NF90) and two pumps having different maximum pressure limits (SQFlex 0.6-3 N, 20 bar; and SQFlex 0.6-2 N, 12 bar), using real-world SI data from a very cloudy day – characterised by different levels of PV power fluctuations. The results were compared against corresponding operations under SOW boundary conditions (without shutdown control), serving as a reference case for evaluating the R-SOW performance.

With SQFlex 0.6-3 N pump, BW30 membrane operating at ~11 bar *TMP* sustained ~67% shutdown resilience and an average *SEC* of ~4.0 Wh/L, while the NF90 membrane which operated at ~9 bar to confine to similar boundary condition, achieved 100% resilience at a *SEC* of ~2.3 Wh/L. The remaining BW30 shutdowns occurred when PV power dropped below the minimum operating threshold of the pump (~150 W). The daily production gains compared to SOW operation were ~ 8 L (BW30) and ~ 19 L (NF90). It was observed that PV-membrane system operation at lower *TMP* (e.g. NF90 vs. BW30) could improve the system resilience during transient operation, as lower *TMP* operation reduces the system power demand and thus lower the $\mathscr{D}_{\mathscr{M}}$ of the pump during low power condition.

Additionally, the operation of two pumps with different maximum pressure limits (0.6-2 N pump, 12 bar; and SQFlex 0.6-3 N, 20 bar) where operated and compared for the membranes under the same operating *TMP* (~11 bar). The investigation with BW30 shows that that the low-pressure pump (SQFlex 0.6-2 N) achieved improved resilience (7 shutdowns vs. 9 for the 0.6–3 N) under the same SOW conditions. Under R-SOW operation, all shutdowns for this pump were eliminated, which also indicate that lower operating pressure can enhance resilience under low and fluctuating PV power conditions.

The use of high-pressure pump (0.6-3 N) could increase the daily production, particularly with NF90 membrane due to higher flux, however it also risked exceeding the "safe" recovery limit during high-power conditions as *TMP* increased. Thus all investigations were conducted at a safe recommended recovery of ≤30% recovery. Moreover, high recovery levels increase the system's *TMP* demand and this increases the susceptibility to shutdowns during transient PV operation, as lower pressure operation has been shown to enhance the system resilience.

Overall, this study presents the methodology for identifying resilience regions of PV-membrane system under real-world transient

conditions and demonstrating its feasibility across different membrane–pump configurations. Operating within the R-SOW can help to improve the system robustness, however since most real-word data points hardly fall within the R-SOW region, back-pressure control strategy has been shown to be effective in mitigating the possible shutdowns and enhance the system resilience, thus improving the reliability of autonomous PV-membrane system without additional energy buffering support.

CRediT authorship contribution statement

Emmanuel Ogunniyi: Conceptualisation, Methodology, Investigation, Software, Validation, Visualisation, Formal analysis, Original draft preparation.

Bryce S. Richards: Conceptualisation, Formal analysis, Methodology, Supervision, Resources, Visualisation, Writing- Reviewing and Editing, Project administration, Funding acquisition.

Declaration of competing interest

The authors declare that they have no known competing financial interests or personal relationships that could have appeared to influence the work reported in this paper.

Acknowledgements

The authors would like to acknowledge: the PhD scholarship for Emmanuel Ogunniyi provided by the Deutscher Akademischer Austauschdienst (DAAD); Martin Ansong (University of Nairobi) for his support during system installation and experimental setup; Hannah Afolayan (Friedrich-Schiller-Universität Jena) for valuable contributions towards the investigation of Sensitivity Analysis. Bryce Richards gratefully acknowledges funding from the Helmholtz Association via the MTET (Materials and Technologies for the Energy Transition) program – Topic 1 – Photovoltaics (38.01.04), and the professorial recruitment initiative.

Appendix A. Supplementary data

Supplementary data to this article can be found online at https://doi.org/10.1016/j.desal.2026.119942.

Data availability

Data will be made available on request.

References

[1] K. Mathew, S. Dallas, G. Ho, M. Anda, A solar-powered village water supply system from brackish water, in: World Renewable Energy Congress VI, Elsevier, 2000, pp. 2061–2064.
[2] W. Ali, H. Farooq, A.u. Rehman, Q. Awais, M. Jamil, A.H.S. Noman, Design considerations of stand-alone solar photovoltaic systems, in: 2018 International Conference on Computing, Electronic and Electrical Engineering (ICE Cube), 2018, pp. 1–6.
[3] E.O. Ogunniyi, B.S. Richards, Photovoltaic power load-matching challenge in a reverse osmosis water desalination system, in: 2024 IEEE PES/IAS PowerAfrica, IEEE, 2024, pp. 1–5.
[4] World Health Organization, Guidelines for Drinking-water Quality 1, World health organization, 2004.
[5] P. Feron, The use of windpower in autonomous reverse osmosis seawater desalination, Wind Eng. (1985) 180–199.
[6] B.S. Richards, G.L. Park, T. Pietzsch, A.I. Schäfer, Renewable energy powered membrane technology: Safe operating window of a brackish water desalination system, J. Membr. Sci. 468 (2014) 400–409.
[7] A. Ruiz-García, I. Nuez, Simulation-based assessment of safe operating windows and optimization in full-scale seawater reverse osmosis systems, Desalination 533 (2022) 115768.
[8] R. Pohl, M. Kaltschmitt, R. Holländer, Investigation of different operational strategies for the variable operation of a simple reverse osmosis unit, Desalination 249 (3) (2009) 1280–1287.
[9] S. Kremen, M. Wilf, P. Lange, Operating results and economics of single stage and two stage large size sea water RO systems, Desalination 82 (1–3) (1991) 3–13.
[10] Q.J. Wei, R.K. McGovern, Saving energy with an optimized two-stage reverse osmosis system, Environ. Sci.: Water Res. Technol. 3 (4) (2017) 659–670.
[11] J. Kim, K. Park, S. Hong, Optimization of two-stage seawater reverse osmosis membrane processes with practical design aspects for improving energy efficiency, J. Membr. Sci. 601 (2020) 117889.
[12] DuPont, FilmTec™ Reverse Osmosis Membranes Technical Manual. https://www.dupont.com/content/dam/water/amer/us/en/water/public/documents/en/RO-NF-FilmTec-Manual-45-D01504-en.pdf, 2025 (accessed 11.27.2025).
[13] R.W. Field, G.K. Pearce, Critical, sustainable and threshold fluxes for membrane filtration with water industry applications, Adv. Colloid Interf. Sci. 164 (1–2) (2011) 38–44.
[14] C. Jun, K. Aghasadeghi, G.T. Daigger, Optimizing air scouring energy for sustainable membrane bioreactor operation by characterizing the combination of factors leading to threshold limiting conditions, Membranes 14 (3) (2024) 58.
[15] R. Xu, Y. Fan, M. Yang, J. Song, Determination of Sustainable Critical Flux through a Long-Term Membrane Resistance Model, Polymers 15 (10) (2023) 2319.
[16] S. Li, Y.-H. Cai, A.I. Schäfer, B.S. Richards, Renewable energy powered membrane technology: a review of the reliability of photovoltaic-powered membrane system components for brackish water desalination, Appl. Energy 253 (2019) 113524.
[17] M. Volk, Pump Characteristics and Applications, CRC Press, 2013.
[18] H. Zhao, X. Zhou, L. Meng, X. Zhu, C. Mou, P. Zhou, Advances in flow control methods for pump-stall suppression: Passive and active approaches, Energies 17 (23) (2024) 6157.
[19] K. Muralidhar, N. Rajasekar, A review of various components of solar water-pumping system: Configuration, characteristics, and performance, Int. Trans. Electr. Energ. Syst. 31 (9) (2021) e13002.
[20] E.M. Salilih, Y.T. Birhane, S.H. Arshi, Performance analysis of DC type variable speed solar pumping system under various pumping heads, Sol. Energy 208 (2020) 1039–1047.
[21] S. Li, A. Voigt, A.I. Schäfer, B.S. Richards, Renewable energy powered membrane technology: energy buffering control system for improved resilience to periodic fluctuations of solar irradiance, Renew. Energy 149 (2020) 877–889.
[22] J. Shen, A. Jeihanipour, B.S. Richards, A.I. Schäfer, Renewable energy powered membrane technology: Experimental investigation of system performance with variable module size and fluctuating energy, Sep. Purif. Technol. 221 (2019) 64–73.
[23] E. Ogunniyi, B.S. Richards, Renewable energy powered membrane technology: Power control management for enhanced photovoltaic-membrane system performance across multiple solar days, Appl. Energy 371 (2024) 123624.
[24] A. Belkaid, I. Colak, O. Isik, Photovoltaic maximum power point tracking under fast varying of solar radiation, Appl. Energy 179 (2016) 523–530.
[25] Grundfos, SQFlex 0.6-2N, 2025. https://product-selection.grundfos.com/de/products/SQFlex/sqf-06-2-n-95027417?pumpsystemid=2786477083&tab=variant-curves. (Accessed 10 October 2025).
[26] Grundfos, SQFlex 0.6-3N, 2025. https://product-selection.grundfos.com/ch/products/SQFlex/sqf-06-3-n-99612442?pumpsystemid=2786469428&tab=variant-curves. (Accessed 10 October 2025).
[27] S. Chandel, M.N. Naik, R. Chandel, Review of solar photovoltaic water pumping system technology for irrigation and community drinking water supplies, Renew. Sust. Energ. Rev. 49 (2015) 1084–1099.
[28] B.S. Richards, G.L. Park, T. Pietzsch, A.I. Schäfer, Renewable energy powered membrane technology: Brackish water desalination system operated using real wind fluctuations and energy buffering, J. Membr. Sci. 468 (2014) 224–232.
[29] A.I. Schäfer, G. Hughes, B.S. Richards, Renewable energy powered membrane technology: A leapfrog approach to rural water treatment in developing countries? Renew. Sust. Energ. Rev. 40 (2014) 542–556.
[30] E.O. Ogunniyi, B.S. Richards, Renewable energy powered membrane technology: electro-hydraulic control system design for managing pump shutdowns in a photovoltaic-membrane water desalination system, Desalination 608 (2025) 118784.
[31] A. Sangwongwanich, Y. Yang, F. Blaabjerg, A cost-effective power ramp-rate control strategy for single-phase two-stage grid-connected photovoltaic systems, in: 2016 IEEE Energy Conversion Congress and Exposition (ECCE), IEEE, 2016, pp. 1–7.
[32] J. Martins, S. Spataru, D. Sera, D.-I. Stroe, A. Lashab, Comparative study of ramp-rate control algorithms for PV with energy storage systems, Energies 12 (7) (2019) 1342.
[33] V.N.X. Que, D. Van Tuan, N.N. Huy, V. Le Phu, Design and performance of small-scale reverse osmosis desalination for brackish water powered by photovoltaic units: a review, in: IOP Conference Series: Earth and Environmental Science vol. 652, no. 1, IOP Publishing, 2021, p. 12024.
[34] M. Freire-Gormaly, A.M. Bilton, Design of photovoltaic powered reverse osmosis desalination systems considering membrane fouling caused by intermittent operation, Renew. Energy 135 (2019) 108–121.
[35] M. Alshawaf, N.S. Alhajeri, Renewable energy-driven desalination for sustainable water production in the Middle East, Int. J. Sustain. Eng. 17 (1) (2024) 668–678.
[36] J. Leijon, D. Salar, J. Engström, M. Leijon, C. Boström, Variable renewable energy sources for powering reverse osmosis desalination, with a case study of wave powered desalination for Kilifi, Kenya, Desalination 494 (2020) 114669.
[37] B.S. Richards, D.P. Capão, W.G. Früh, A.I. Schäfer, Renewable energy powered membrane technology: Impact of solar irradiance fluctuations on performance of a brackish water reverse osmosis system, Sep. Purif. Technol. 156 (2015) 379–390.
[38] Y.-A. Boussouga, B.S. Richards, A.I. Schäfer, Renewable energy powered membrane technology: System resilience under solar irradiance fluctuations during

the treatment of fluoride-rich natural waters by different nanofiltration/reverse osmosis membranes, J. Membr. Sci. 617 (2021) 118452.
[39] P. Gasser, et al., A review on resilience assessment of energy systems, Sustain. Resilient Infrastruct. 6 (5) (2021) 273–299.
[40] Dupont, Filmtech BW30–4040 membrane Technical manual, 2025. https://www.lenntech.com/Data-sheets/Dow-Filmtec-BW30-4040.pdf. (Accessed 5 May 2025).
[41] A. Alexiadis, J. Bao, D. Fletcher, D. Wiley, D. Clements, Analysis of the dynamic response of a reverse osmosis membrane to time-dependent transmembrane pressure variation, Ind. Eng. Chem. Res. 44 (20) (2005) 7823–7834.
[42] G.L. Park, A.I. Schäfer, B.S. Richards, Renewable energy powered membrane technology: The effect of wind speed fluctuations on the performance of a wind-powered membrane system for brackish water desalination, J. Membr. Sci. 370 (1–2) (2011) 34–44.
[43] H.R. Lotfy, J. Staš, H. Roubík, Renewable energy powered membrane desalination—review of recent development, Environ. Sci. Pollut. Res. (2022) 1–17.
[44] M. Alghoul, P. Poovanaesvaran, K. Sopian, M. Sulaiman, Review of brackish water reverse osmosis (BWRO) system designs, Renew. Sust. Energ. Rev. 13 (9) (2009) 2661–2667.
[45] Y.-H. Cai, Y.-A. Boussouga, A.I. Schäfer, Renewable energy powered membrane technology: Impact of intermittency on membrane integrity, Desalination 580 (2024) 117504.